Quaternary Research (2021), **103**, 113–129
doi:10.1017/qua.2020.115

Research Article

Evidence from the Dayao Paleolithic site, Inner Mongolia for human migration into arid northwest China during mid-Pleistocene interglacials

Junyi Ge[a,b,c*], Yinghua Wang[d], Mingchao Shan[d], Xingwu Feng[a], Fuyou Chen[a], Haibin Wu[b,c,e], Qin Li[e], Xinying Zhou[a,b,c], Yan Li[f], Ruiping Tang[c], John W. Olsen[a,g], Chenglong Deng[c,h] and Xing Gao[a,b,c]

[a]Key Laboratory of Vertebrate Evolution and Human Origins, Institute of Vertebrate Paleontology and Paleoanthropology, Chinese Academy of Sciences, Beijing, China; [b]CAS Center for Excellence in Life and Paleoenvironment, Beijing, China; [c]University of the Chinese Academy of Sciences, Beijing, China; [d]Inner Mongolia Museum, Hohhot, China; [e]Key Laboratory of Cenozoic Geology and Environment, Institute of Geology and Geophysics, Chinese Academy of Sciences, Beijing, China; [f]School of Ocean Sciences, China University of Geosciences (Beijing), Beijing, China; [g]School of Anthropology, University of Arizona, Tucson, USA and [h]State Key Laboratory of Lithospheric Evolution, Institute of Geology and Geophysics, Chinese Academy of Sciences, Beijing, China

Abstract

The Dayao Paleolithic site, located in Inner Mongolia on the eastern margin of China's vast northwestern drylands, was a lithic quarry-workshop utilized by Pleistocene human migrants through the region. Determining the age of this activity has previously yielded controversial results. Our magnetostratigraphic and OSL dating results suggest the two artifact-bearing paleosols are correlated with MIS 5 and 7, respectively. Correlating paleoclimatic data with marine $\delta^{18}O$ records leads us to conclude that two sandy gravel layers containing many artifacts in the lower part of the Dayao sequence were formed during MIS 9 and 11, if not earlier. Our results reveal that the earliest human occupation at the Dayao site occurred before ca. 400 ka during a relatively warm and moist interglacial period, similar to several subsequent occupations, documenting the earliest and northernmost archaeological assemblage yet reported in China's arid northwest. We conclude that the northward and southward displacements of the East Asian summer monsoon rain belt during past interglacial-glacial cycles were responsible for the discontinuous human occupation detected at the Dayao site. The penetration of this precipitation regime into dryland ecologies via the Huanghe (Yellow River) Valley effectively created a corridor for hominin migration into China's arid northwest.

Keywords: Glacial-interglacial cycles, Paleoclimatic reconstruction, Hominin occupation, Paleolithic demography, Green corridor

(Received 12 June 2020; accepted 10 November 2020)

INTRODUCTION

Between ca. 1.2–0.5 Ma, spanning the Early–Middle Pleistocene boundary, the Earth's climate underwent a fundamental change called the Mid-Pleistocene Transition (MPT), which profoundly affected oceanic and atmospheric circulation, the growth and decline of ice sheets, and the distribution and evolution of biota, including the ancestors of modern humans (Head et al., 2008). During this transition, the low-amplitude, 41 ka, obliquity-driven climatic cycles of the earlier Pleistocene were progressively overshadowed by ~100 periodic, low frequency fluctuations (Clark et al., 2006; Imbrie et al., 1993), leading to greatly increased climate contrasts between glacial and interglacial periods, including a succession of severe glacial episodes, particularly in the Northern Hemisphere.

These amplified glacial-interglacial climatic changes and subsequent prolonged and extremely cold glacial environments significantly influenced hominin evolution and migration, especially in the higher northern latitudes of Eurasia. Some authors have proposed that extreme climatic conditions in glacial periods may have led to the local extirpation of human populations in northern high-latitude areas of Eurasia, as indicated by significant hiatuses in the presence of middle Pleistocene hominins during the pleniglacial climatic conditions of Marine Isotope Stage (MIS) 4, as well as earlier cold periods, such as MIS 6 (Hublin and Roebroeks, 2009). Other authors have argued that contraction of habitable areas during cold glacial periods may have driven human populations to focus on preferred habitats and become displaced into southern refugia where they "overwintered," escaping cold climatic conditions, and recolonized the north only when environmental conditions ameliorated (Dennell, 2003; Stewart and Stringer, 2012). This "ebb and flow" model has also been proposed as an explanation for patterns of human occupation and migration in North China (Dennell, 2003). According to this model, humans nearly abandoned their preferred habitats established during warm and wet interglacial periods in northern China (Dennell, 2003), moving south to areas such as the Qinling Mountains (Sun et al., 2017) due to much colder and drier climatic conditions and the large-scale advance of deserts during glacial periods, thus creating a discontinuous record of human occupation in North China (Dennell, 2013a). However, new $^{26}Al/^{10}Be$ studies of the absolute antiquity

*Corresponding author: (J. Ge) gejunyi@ivpp.ac.cn

Cite this article: Ge J *et al* (2021). Evidence from the Dayao Paleolithic site, Inner Mongolia for human migration into arid northwest China during mid-Pleistocene interglacials. *Quaternary Research* **103**, 113–129. https://doi.org/10.1017/qua.2020.115

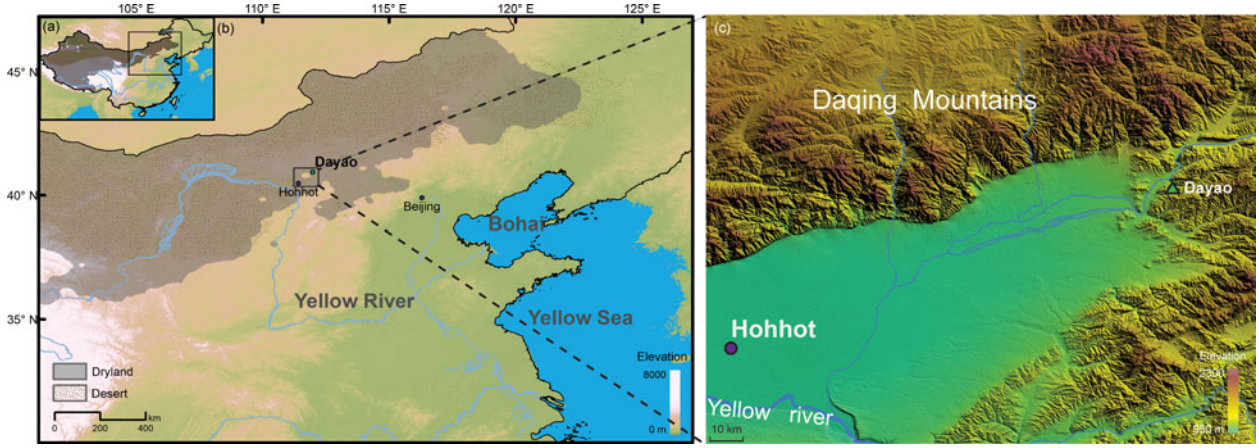

Figure 1. Location map of the Dayao site. Green triangle on map (c) indicates the excavation location. (For interpretation of the references to color in this figure legend, the reader is referred to the web version of this article.)

of *Homo erectus* at Zhoukoudian reveal a hominin presence in northern China throughout a cold but relatively mild glacial period corresponding to MIS 18 (Shen et al., 2009). Thus, the question of whether and how human ancestors survived glacial periods in residence in North China is still open to debate.

Today, Asia includes ~32% of global arid climates, ~6,000,000 km^2 of which consists of true deserts (Thomas, 2011). As a result of the uplift of the Tibetan Plateau and its consequent blocking of moisture generated by summer monsoon activity, vast areas of arid and semi-arid climates, including the Gobi Desert, have developed in the inland regions north of Tibet (i.e., North China), since the late Cenozoic (Guo et al., 2008). These widespread drylands in continental Asia may have profoundly affected the course of hominin evolution in the region and the nature of human settlement patterns and technologies. For example, increasing aridification during the middle Pleistocene may have impeded human migration across Eurasia and possibly led to the isolation of *H. erectus* in China from its counterparts in Central Asia (Dennell, 2013b). During some middle Pleistocene interglacial intervals, especially those from MIS 15 to MIS 11 (ca. 580–380 ka), greatly increased temperatures and rainfall may have provided opportunities for human ancestors and faunas to disperse into China from the west (Dennell, 2016), possibly facilitating the spread of some populations of *Homo heidelbergensis* into East Asia (Rightmire, 1998, 2001). Hao et al. (2015) even suggested that the very long periods of interglacial climate in the northern hemisphere during MIS 15–13 created favorable conditions for the second major dispersal of African hominins into Eurasia. However, due to the paucity of securely dated Paleolithic archaeological assemblages, the extent to which human ancestors successfully adapted to dryland environments in northern China during the middle Pleistocene is still poorly understood.

We report here on investigations of the Dayao Paleolithic site in Inner Mongolia, located on the margin of China's extensive northwest arid lands. Due to fluctuations in the East Asian summer monsoon regime during Pleistocene glacial and interglacial periods, these arid lands expanded and contracted accordingly, as witnessed by alternating changes in grain sizes of paleosol and loess layers on the Chinese Loess Plateau (Ding et al., 2002). Therefore, the Dayao Paleolithic site constitutes an ideal record for examining ancient human adaptations to dryland environmental changes in North China in response to glacial-interglacial climate changes. We employed multiple dating methods in this study, including magnetostratigraphy, Optically Stimulated Luminescence (OSL), and climatostratigraphy, applied for the first time at Dayao, to clarify the age and sequence of human occupation. We then quantitatively reconstructed paleoclimatic changes through pollen analysis to explore the influences of those changes on human occupation of the site.

GEOLOGICAL AND ARCHAEOLOGICAL SETTINGS

The Dayao Paleolithic site (40°56′N, 111°80′E) is located northeast of the Hetao (Ordos) fluvial plain that extends along the northern bank of the Huanghe (Yellow River) at its Great Bend, ~20 km northeast of Hohhot, the capital of China's Inner Mongolia Autonomous Region (Fig. 1). The site lies on the second terrace of the Dayao River, which originates on the southern piedmont of the Daqing Mountains and flows south to the Yellow River plain. The site was discovered in 1973 and excavated first from 1979–1983 (Wang and Olsen, 1985). Additional excavations were conducted at the site between 2013–2015.

A sediment sequence ~16 m thick is exposed at the Dayao site on the north side of an east-west trending gully where the stratigraphic sequence can be visually divided into three components from top to bottom (Fig. 2a, b). The upper unit is composed of coupled loess-paleosol layers ~6.5 m thick, with a red-brown paleosol layer underlying a thick, pale-yellow loess stratum. Within this upper loess layer (0–5.5 m), a thin horizon of coarse sand is interbedded between 0.8 m and 1.2 m in depth with rounded and sorted calcareous nodules distributed at the bottom, possibly suggesting an erosional event under relatively cold climatic conditions. The middle unit, varying between 6.5 m to ~12 m in thickness, comprises a sequence of yellowish loess-like sediments and interbedded red-brown paleosol layers, which are rather similar to those in the upper unit, indicating that they may also originate from eolian dust, somewhat reworked by water. A paleosol occurs in this unit at depths between ~8.8 m to ~10.2 m, and exhibits apparent features of gleying. In addition, a few small angular brecciated inclusions, transported a short distance from nearby Dayao Hill by slopewash or gravity, were observed, indicating that this sequence was affected by groundwater variations and slope processes. Beneath the middle unit, a massive bedrock block was exposed

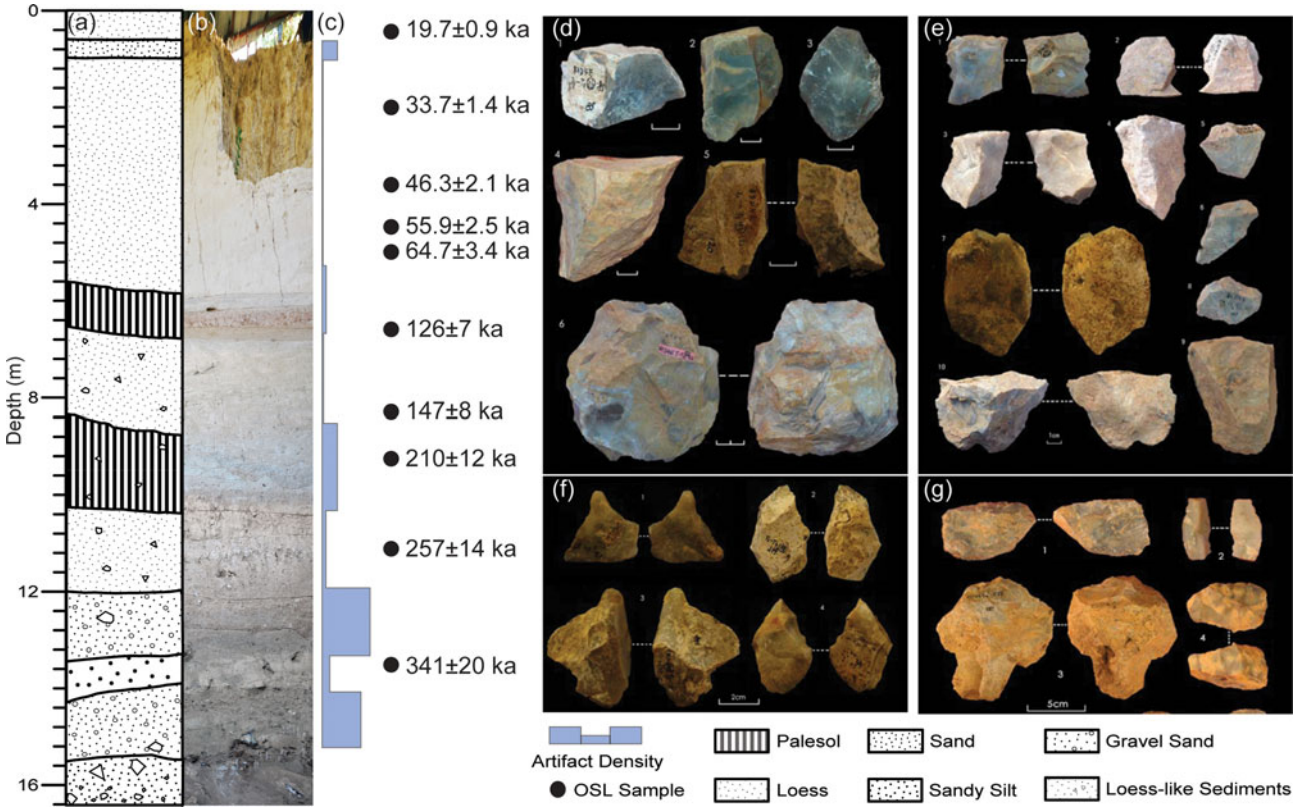

Figure 2. (color online) The lithostratigraphic sequence (a, b) and OSL ages, variations in Paleolithic artifacts throughout the sediment sequence (c), and (d–g) representative artifact types from the Dayao site. The solid circles correspond to the position of OSL samples. (d)–(g) Representative Paleolithic cores, flakes, points, and scrapers from the Dayao site, respectively.

in the eastern portion of the excavation square. In this sedimentary sequence, it was observed that deposition of the middle and upper units was influenced by underlying massive bedrock, where overlying sedimentary and paleosol strata are inclined with respect to the level of the bedrock. Slope angles decrease with increasing distance from the exposed bedrock, providing further evidence of the eolian origin of those sediments.

The lower unit, occurring behind the massive bedrock block, mainly comprises a thick sequence of fluvial and slope-wash deposits dominated by gravel and sand, occasionally including large breccia fragments. The gravels included in this horizon are mostly sub-angular and sub-rounded, and moderately sorted, suggesting they may have been transported by fluvial action near a riverbank. Some horizontal sandy laminations were also observed in the field. Based upon grain size and sedimentary features, this sediment sequence can be further divided into four sub-layers: (1) grayish-brown gravel and sand containing breccia fragments (12.0–13.5 m), in which some thin horizontal sandy laminations were visible; (2) a layer of gravel and sandy silt between ~13.5 m and ~14.4 m deep; (3) yellow-brown laminated gravel and sand layers with a thickness of 1.5 m; and (4) brown gravel and sand, including breccia fragments, in which the lower sub-layer's grain size and proportion of gravel gradually increase downward.

To date, more than 3000 artifacts have been unearthed at this locality during two excavation campaigns, including 455 artifacts yielded by carefully controlled excavations undertaken in 2013–2015 in the ~16-m-thick sediment sequence at Dayao. To accurately evaluate artifact distribution density, we calculated the average abundance of artifacts in various sedimentary strata by dividing the total number of the artifacts unearthed from each unit by its thickness, based on the sample of artifacts yielded by recent excavations. Our results (Fig. 2c) indicate that artifacts occur mostly in the lower unit, especially in the two gravel-sand layers, but are scarce in the interbedded sandy silt layer. In the middle and upper units, however, artifacts occur mainly in paleosol layers, and are nearly absent from most of the loess strata. Thereafter, the subsequent analyses of pollen and other proxies are mainly concentrated on the lower part of the Dayao section where the artifacts occur. It is worth noting that a small density peak of artifacts occurred in the coarse-sand unit between 0.8 m and 1.2 m deep, possibly resulting from intensive surface erosion that washed out fine materials leaving larger, heavier artifacts in situ.

The artifacts discovered at the Dayao site are made mostly on locally outcropping chert, and are mainly comprised of chunks, cores, complete and incomplete flakes, and retouched tools typologically classified as scrapers, burins, points, borers, and chopper-chopping tools (Fig. 2d). Close examination of these artifacts indicates that most were never used as tools by human ancestors, suggesting this site functioned primarily as a quarry-workshop for the production of artifacts that were then transported and used off-site (Feng, 2008).

The present climate of the Dayao area is semi-arid (Köppen-Geiger BWk), with average annual precipitation and temperature values of 390 mm and 5°C, respectively. Modern vegetation in this area is dominated by perennial low-temperature herbaceous xerophytes, such as *Artemisia* sp. and members of the Compositae and Gramineae (Poaceae) families, with some natural secondary forests and, now, artificial woodlands dominated by *Betula*, *Populus*, *Quercus*, *Pinus tabulaeformis*, and *Picea asperata* on hills and mountainsides.

SAMPLING AND EXPERIMENTAL METHODS

Paleomagnetic measurements

Fifty-eight oriented block samples were collected at 20–40 cm intervals along the Dayao section. In the laboratory, samples were cut into standard 2×2×2 cm cubic specimens for paleomagnetic measurements. To establish a reliable magnetic polarity profile, all specimens were subjected to stepwise thermal demagnetization up to 610°C in 15 steps and 10–50°C increments using an ASC Scientific TD-48 thermal demagnetizer. The characteristic remnant magnetization (ChRM) was isolated after removal of a soft secondary component of magnetization. Remanence measurements were made using a 2 G Enterprises 760-R cryogenic magnetometer installed in a magnetically shielded space with a background field of <300 nT. All experiments were conducted in the Palaeomagnetism and Geochronology Laboratory of the Institute of Geology and Geophysics of the Chinese Academy of Sciences in Beijing.

Optically Stimulated Luminescence (OSL) determinations

During excavations, ten OSL samples were collected from the Dayao sequence above ~13.5 m depth to provide further age constraints. All OSL samples were obtained by hammering steel tubes (25-cm-long cylinders with a diameter of 5 cm) into a freshly dug vertical section. The tubes were then covered and sealed with aluminum foil, wrapped in black plastic bags and taped shut to avoid light exposure and moisture loss. The OSL dating samples were prepared under subdued red light. The sediment from the sunlight-exposed end of the cylinder was separated and used for dose rate and water content measurements, and the material from the middle of the cylinder was wet-sieved to obtain the coarse-grain (CG, 63–90 μm and 90–150 μm) fractions, followed by treatment with 30% hydrogen peroxide (H_2O_2) and 10% hydrochloric acid (HCl) to remove organic matter and carbonates, respectively. The quartz-rich and potassium feldspar-rich (K-feldspar) fractions were then separated with a heavy liquid (sodium polytungstate, $HNa_6O_{40}W_{12}$) solution of 2.58 g/cm^3 and 2.62 g/cm^3, separately. Finally, these prepared quartz-rich fractions were etched with 40% hydrofluoric acid (HF) for 3600 s, followed by a 10% HCl rinse, to remove the outer alpha-irradiated surface of the quartz grains and to eliminate any potential feldspathic contamination. The purity of the isolated quartz was checked by calculating the ratio of Infrared Stimulated Luminescence (IRSL) to OSL and the characteristic 110°C TL peak of quartz. Samples with obvious IRSL signals were re-treated until the OSL-IR depletion ratio was uniform within 10%. The separated quartz grains were then mounted as monolayers onto 9.7-mm-diameter steel discs using silicone oil adhesive (sample diameter, 1 mm). In this study, both quartz and K-feldspar OSL signals were employed to determine the ages of the samples.

All luminescence measurements were made with an automated Risø Model DA-20 TL/OSL readers equipped with a $^{90}Sr/^{90}Y$ beta source for irradiation (Bøtter-Jensen et al., 2003) and an EMI 9235QA photomultiplier tube. Blue light LED (470 ± 30 nm) stimulation set at 90% of 50 mW/cm^2 full power and 7.5 mm Hoya U-340 filters (transmission between 290 nm and 370 nm) were used for the quartz OSL measurements. Coarse-grained K-feldspar was stimulated with infrared (IR) diodes emitting at 870 nm (90% of 280 mW/cm^2), and a combination of Schott BG39 and Corning 7–59 filters (transmission 320–460 nm) was used to detect the luminescence signals.

The quartz D_e value was determined using a standard SAR protocol (Table 1a; Murray and Wintle, 2000, 2003). The OSL signals from the first 0.4 s of optical stimulation time, which are dominated by the fast component, were used to determine the equivalent dose (Smith and Rhodes, 1994; Jain et al., 2003; Wintle and Murray, 2006). The dose response curve was fitted using the one saturating exponential function. Prior to quartz D_e measurement, dose recovery and preheat plateau tests were conducted to determine the most appropriate setting of thermal treatment in the SAR protocol for the studied samples. The preheat temperature varied from 160°C to 300°C in 20°C increments, with three aliquots measured at each temperature. The tracked cut-heat model suggested by Roberts (2006) was applied, which uses a cut-heat temperature 40°C lower than the corresponding preheat temperature. For the preheat plateau test, the mean D_e value of the three aliquots was calculated for each preheat temperature. A dose recovery test for coarse quartz using the SAR protocol outlined in Table 1a was carried out on five samples with given doses ranging between 55–190 Gy. Three aliquots for each sample were first bleached, and the fixed given dose was applied. The dose recovery ratio was determined by dividing the obtained D_e by the given dose. Feldspar measurements employed a pIRIR290 protocol (Table 1b; Buylaert et al., 2012; Yi et al., 2016), with preheat and cut-heat at 320°C for 60 s, and a second IR stimulation temperature at 290°C. Cleanout at the end of each SAR cycle was at 325°C with IR stimulation (all IR stimulations lasted 200 s). For quartz, the first 0.3 s integral after early background subtraction from the following 1.7 s was used for calculation (Cunningham and Wallinga, 2010). For feldspar, the first 2 s of the post-IR IRSL signal minus a background estimated from the last 50 s was used.

Concentrations of uranium (U), thorium (Th), and potassium (K) in ten samples were measured by Neutron Activation Analysis (NAA). The in situ water content (moist mass/dry mass) was determined by weighing the sample before and after drying, and was assigned an absolute uncertainty of ± 5%. Using the revised dose rate conversion factors of Guérin et al. (2011) and water content attenuation factors (Aitken, 1985), the elemental concentrations were converted into an effective dose rate. The cosmic ray dose rate was estimated for each sample as a function of depth, geographical elevation, and geomagnetic latitude, following Prescott and Hutton (1994). K-feldspar grains have an internal radioactivity due to the presence of ^{40}K in their crystal structure. Assumed K-feldspar dose rates with K and Rb concentrations of 12.5 ± 0.5% and 400 ± 100 ppm, respectively, were therefore used for internal dose-rate calculations (Huntley and Baril, 1997). Alpha efficiency values (a-value) of 0.08 ± 0.02 for K-feldspar (Rees-Jones, 1995) were used. Finally, dose rates and ages were calculated using DRAC software (Durcan et al., 2015).

Palynological analysis

Thirty sediment samples taken at 20-cm intervals were collected between 10.8 m and 16.5 m depth in the Dayao section for palynological analysis, in order to reconstruct glacial-interglacial climatic changes recorded by the coarse-gravel and sand sediments. Pollen grains and spores were extracted using the acid-alkali-free method (Moore et al., 1991). For each sample, ~80 g of sediment were first treated with HCl (15%) and NaOH (~3%) to remove carbonates and organic matter, respectively. Heavy-liquid separation with a zinc chloride ($ZnCl_2$) solution (specific density 1.8 g/cm^3) was used to concentrate the pollen. Finally, silicates were removed

Table 1. Quartz OSL and K-feldspar pIRIR290 equivalent dose measurement protocols used in this study: (a) Quartz OSL protocol after Murray and Wintle (2003); (b) Post-IR IRSL protocol from Buylaert et al. (2012). For the "natural" sample, i = 0 and $D_0 = 0$. The sequence is repeated for several regenerative doses, including zero and repeat doses.

Step	(a) SAR protocol	Observed	(b) $pIRIR_{290}$ protocol	Observed
1	Give regenerative dose, D_i		Give regenerative dose, D_i	
2	Preheat (260° C, 10 s)		Preheat (320° C, 60 s)	
3	OSL (125° C, 40 s)	L_X	IRSL (200° C, 200 s)	
4	Test dose		IRSL (290° C, 200 s)	L_X
5	Cut-heat (220° C)		Test dose	
6	OSL (125° C, 40 s)	T_X	Preheat (320° C, 60 s)	
7	Return to step 1		IRSL (200° C, 200 s)	
8			IRSL (290° C, 200 s)	T_X
9			IRSL (325° C, 200 s)	
10			Return to step 1	

using HF (40%) and HCl (30%) before mounting the palynomorphs in glycerin jelly (Faegri and Iversen, 1975). *Lycopodium* tablets were added to the samples to allow estimation of pollen concentrations. About 4,300 pollen grains were identified in 82 processed samples. At least 100 pollen grains were counted in most samples. Morphological keys were used to identify pollen taxa (e.g., Xi and Ning, 1994; Wang et al., 1997). Pollen percentages were calculated from the sums of the arboreal and non-arboreal taxa identified in each pollen spectrum. Pollen data were analyzed and graphically represented using Origin (https://www.originlab.com/) and C2 software packages (https://www.staff.ncl.ac.uk/stephen.juggins/software/C2Home.htm).

Quantitative reconstructions of climatic changes

For better correlation with marine $\delta^{18}O$ records that reflect global climatic changes, we applied the Modern Analog Technique (MAT) (Overpeck et al., 1985; Guiot, 1990; Mu et al., 2015) to quantitatively reconstruct sequences of annual average surface air temperature (ANNT) and annual average precipitation (ANNP) in the Dayao area. Our quantitative paleoclimatic reconstruction employed modern analog technique (MAT) that matches fossil and modern pollen samples using the squared chord distance (SCD) dissimilarity metric to infer paleoclimate from those associated with modern samples that have taxonomic assemblages most similar to each fossil assemblage. Modern pollen data were derived from the East Asian Pollen Database (EAPD) (Zheng et al., 2014). After excluding sites exhibiting obvious human impact, a total of 1756 pollen spectra were included in this study, which covers most regions of China. Modern climate data for pollen sites, including annual average temperature (ANNT) and precipitation (ANNP) were derived from WorldClim climate data (version 2; Fick and Hijmans, 2017) via extraction by R code. The WorldClim data set is interpolated on a 1 km grid by using monthly station climate data (1970–2000) with covariates including elevation, distance to coastlines, and MODIS-derived maximum and minimum land surface temperature and cloud cover, which improve the interpolation accuracy for climate variables.

We applied plant functional types (PFTs) to match the fossil and modern analogues rather than relying on individual taxa, which could reduce the influence of "no analogues" outcomes in the past and anthropogenic factors, since the PFTs represent broad classes of plant groups defined by stature, leaf form, and phenology, thus a better-defined response to climate changes (Prentice et al., 1996). The classification of PFT assignments in China follows the Members of the China Quaternary Pollen Data (MCQPD, 2000), and paleoclimate reconstruction was conducted by means of the PPPbase software package (Guiot and Goeury, 1996).

The accuracy of this approach was evaluated from modern data by comparing reconstructed values with the estimated modern climate at corresponding surface pollen sites. A high coefficient of determination (R^2) between predictions and observations, 0.82 for ANNT and 0.94 for ANNP, indicates the high reliability of this method.

RESULTS

Paleomagnetic analysis

Demagnetization results were evaluated by orthogonal diagrams (Zijderveld, 1967) and the principal component direction was computed by means of principal component analysis (Kirschvink, 1980) on a minimum of four consecutive steps using PaleoMag software (Jones, 2002). For most samples, a secondary magnetic component, probably of viscous origin, was removed by thermal demagnetization at 250–300°C, and the highly stable ChRM component isolated between 300°C and 585–610°C (Fig. 3), indicating that magnetite dominates the remanence carriers.

Among the 58 analyzed samples, 10 were excluded owing to unstable demagnetization trajectories (for example, in cases where it was not possible to isolate the ChRM directions, and/or where the ChRM directions gave a maximum angular deviation (MAD) >15°, or to ChRM directions giving Virtual Geomagnetic Pole (VGP) latitudes more than 45° from the mean VGP, which are regarded as outliers and transitional directions (Kirschvink, 1980). Consequently, 48 samples yielded reliable ChRM directions, and VGP latitudes were calculated from ChRM data to construct the magnetostratigraphy of the Dayao section (Fig. 4). Following demagnetization, only one magnetozone of normal polarity was recognized in this section (Fig. 4). Based on

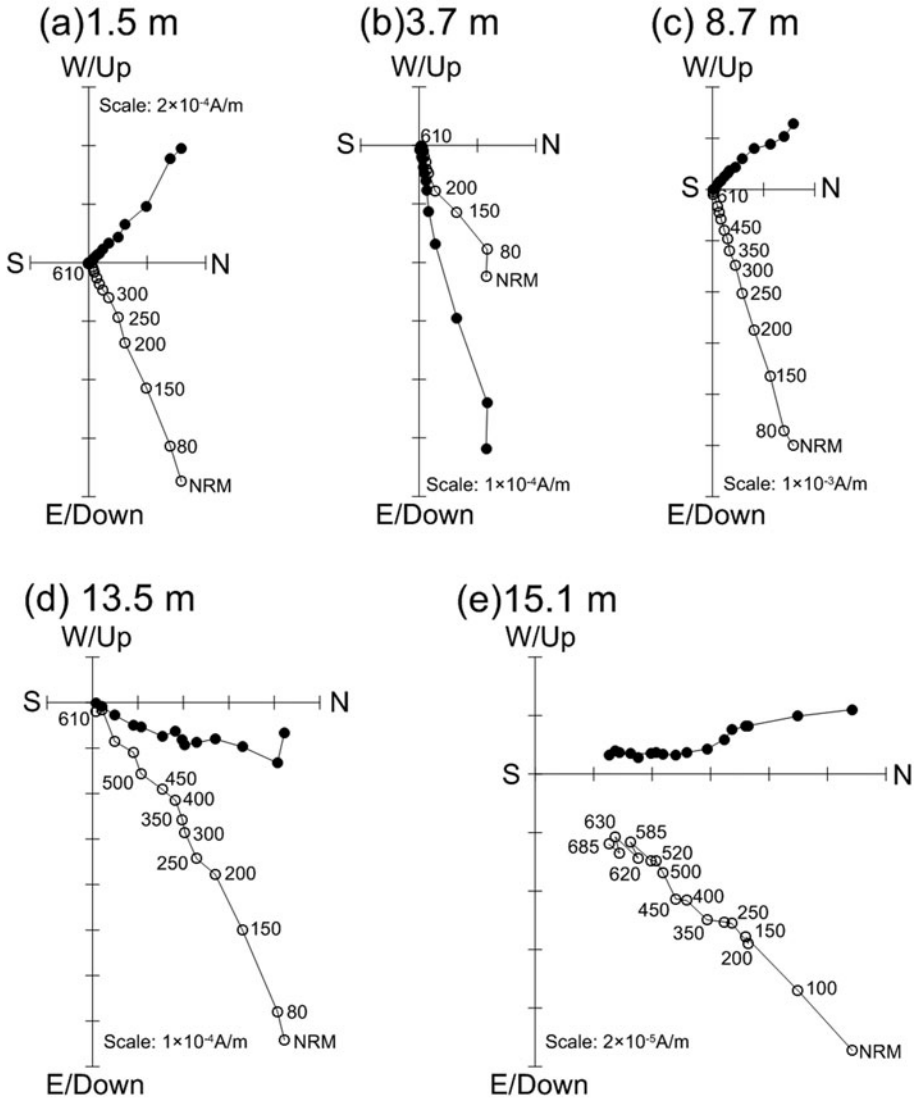

Figure 3. Orthogonal projections of representative progressive thermal demagnetization. The open (solid) circles refer to the vertical (horizontal) planes. The numbers refer to temperatures in degrees Celsius. NRM = natural remnant magnetization.

subsequent OSL dating results covering most of the sequence, which yields an age range of 20–320 ka, we correlate this magnetozone with the Brunhes Normal chron, indicating a *terminus post quem* of ca. 780 ka for the Dayao section.

OSL dating

The results of preheat plateau and dose recovery tests for one representative sample (HED-142) are presented in Figure 5a. It can be seen that over a wide temperature interval between 180–280°C, quartz D_e seem to be independent of varied preheat temperatures, recycling ratios are generally between 0.9 and 1.1, and recuperation values are <5%. The results of the dose recovery test are shown as a measured to given dose plot in Figure 5b. The dose recovery ratios are, overall, within 10% of unity (Fig. 4b), indicating that our SAR protocol was able to measure a quartz dose given prior to any heat treatment at an acceptable degree of accuracy. Therefore, a preheat temperature of 260°C and a cut-heat at 220°C were used for D_e determination of all samples.

Figure 5c shows typical decay and dose-response curves for one representative sample (again, HED-142) from the Dayao section. The recuperation was <5%. The D_e values of the aliquots with recycling ratios of <0.9 or >1.1 were excluded for D_e determination. These features of quartz OSL at the Dayao site are similar to those from typical Chinese loess samples, possibly providing independent evidence of the eolian origin of these Dayao sediments.

Generally, the percentages of aliquots with $2D_0$ values smaller than the average dose (derived from all aliquots) for calculation of the mean D_e were used to assess possible age underestimation. For the upper four samples (<160 Gy), no aliquots meet the criterion. However, in sample HED-144 from a depth of 4.5 m, one out of ten measured aliquots yielded D_e values higher than $2D_0$ and were therefore rejected. Quartz OSL ages of 19.7 ± 0.9—55.9 ± 2.5 ka were obtained on the upper four samples. This is in agreement with the conclusions of previous studies that, typically, age underestimation is observed when doses are higher than 160 Gy in Chinese loess using quartz SAR OSL (Buylaert et al., 2012; Yi et al., 2016). Therefore, we used post-IR IRSL signals, which have been proven more stable compared with conventional IRSL signals measured at ambient temperatures, to date samples obtained below 4.5 m depth in the Dayao sequence. A great deal of evidence has shown that an apparently stable pIRIR signal can be obtained when the first IR stimulation temperature is ≥ 170°C (e.g., Buylaert et al., 2007, 2008; Stevens et al., 2018), and has relatively

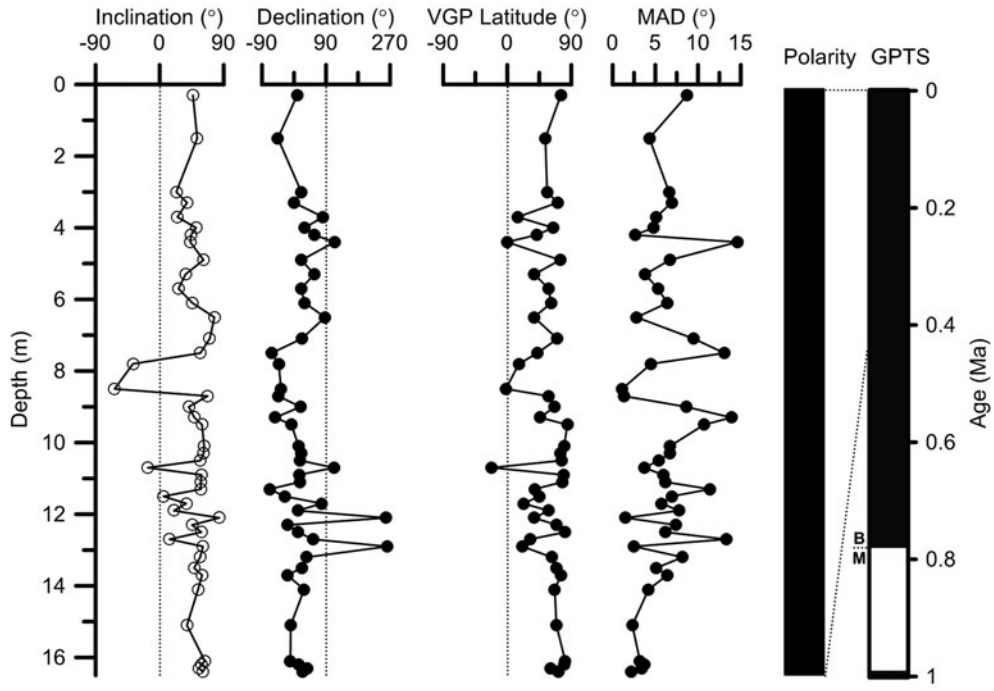

Figure 4. Magnetostratigraphy of the Dayao site and correlations with the geomagnetic polarity timescale (GPTS).

low or nearly negligible fading rates (Yi et al., 2016). Therefore, the $pIRIR_{200, 290}$ protocol was used in this study, with a test dose of 30% of the total dose, which typically generated good dose recovery (Yi et al., 2016). To examine the dependence of the pIRIR dating results on test dose size and evaluate the applicability of our pIRIR protocol, a dose recovery test was carried out using $pIRIR_{200, 290}$ protocols. Figure 5d presents another recovery test on bleached (~300 h in Hönle SOL2 lamp) 90–150 μm feldspar-rich grains from five samples (the test dose was ~30% of dose of interest). The residual doses in these post-bleaching samples were 7 ± 2 Gy (n = 15) on average, and this value was subtracted from the measured doses. For doses up to at least ~1200 Gy, our chosen SAR $pIRIR_{200, 290}$ protocols were able to satisfactorily recover a dose given in the laboratory. The finite pIRIR290 D_e values fall between 187.2 ± 6.1 and 1075 ± 28 Gy, while the lowermost sample (HED-150) yielded an infinite D_e of >1368 Gy, which is beyond the upper dating range determined by 2D0 value. The pIRIR290 age ranged from 126 ± 7 to 257 ± 14 ka, and an infinite age of >341 ka was obtained for sample HED-150.

One fundamental assumption underlying OSL dating is the full resetting of luminescence signals prior to deposition (Aitken, 1985). The D_e distributions from many aliquots of a sample can be used to assess whether the signal has been reset sufficiently prior to deposition (e.g., Olley et al., 1999; Arnold et al., 2007), and the over-dispersion value (σOD), representing the relative standard deviation of the D_e distribution, is often used for measurement uncertainties (Galbraith et al., 1999; Olley et al., 2004). Generally, samples with σOD values of 20% were regarded as undisturbed and bleached uniformly (Olley et al., 2004; Duller, 2008). Dose distributions and relevant statistical characteristics of ten samples are shown in Figure 6. These samples typically describe a normal Gaussian distribution or are only slightly skewed, and all give over-dispersion (σOD) values of <20%, indicating that they are well bleached.

Finally, the central age model (CAM) of Galbraith et al. (1999) was used for D_e calculation of each sample. The results of dose rate calculation as well as OSL ages are listed in Table 2. As shown in Figure 7, most of the Dayao section, especially in the middle and lower parts, exhibits a rather constant and stable sediment accumulation rate (SAR), suggesting a relatively continuous sedimentary sequence without significant hiatus. At ca. 70 ka, a significant increase of SAR was observable, possibly attributing to the much drier and cold climate during the last glacial period, as witnessed by the thick last glacial Malan loess (L1) (Liu et al., 1998; Porter, 2001) in the Chinese Loess Plateau.

Palynological analysis and quantitative reconstructions of regional climatic changes

The percentage pollen spectrum for the Dayao section is illustrated in Figure 8. The results of stratigraphically constrained cluster analysis using swMATH CONISS software are also shown. These data clearly reflect diachronic changes in the woodland and grassland vegetation communities surrounding the site.

In addition to considering the results of the CONISS cluster analysis, zoning of the pollen spectrum emphasizes changes in major representative plant taxa such as *Pinus*, *Betula*, and *Artemisia*, as well as members of the Chenopodiaceae and Asteraceae families that occur in higher proportions in the pollen assemblage. The diagram can be divided into four main pollen assemblage zones, described below.

Pollen Assemblage Zone 4 (Artemisia-*Chenopodiaceae*) *(16.5–15.2 m)*

Pinus pollen appears in low frequencies; other arboreal taxa are not present in this zone. *Artemisia* is the main herbaceous pollen type, averaging more than 80% of the samples. Members of the Chenopodiaceae are also present at high frequencies. Other herbaceous taxa, including members of the Asteraceae and Ranunculaceae families and the genus *Humulus*, appear in low frequencies.

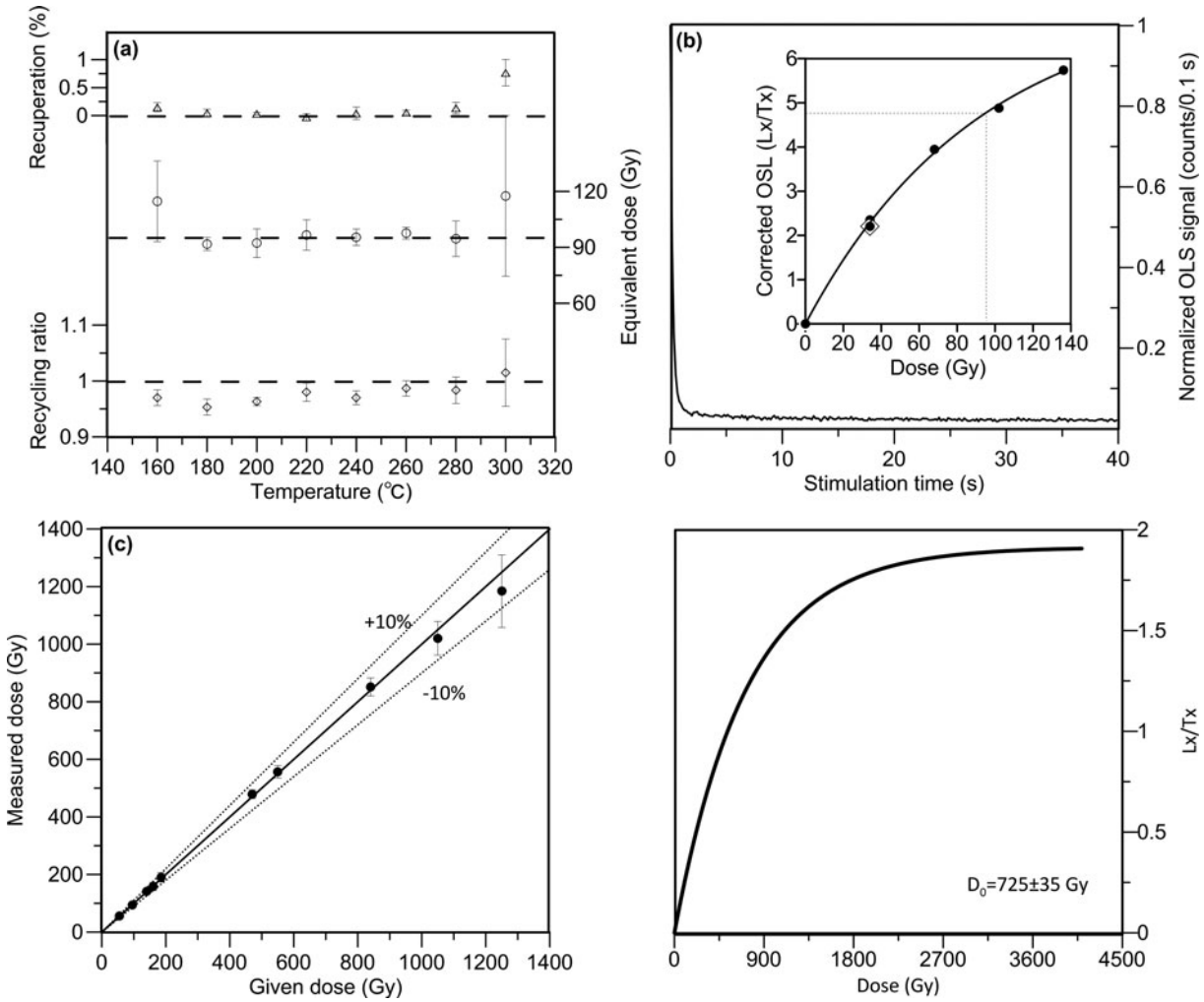

Figure 5. OSL characteristics of Quartz and K-Feldspar from the Dayao site. (a, b) Preheat plateau test, normalized decay curve, and dose response curve (inset) for sample HED-142. (c) Results of dose recovery shown as measured to given dose plot for ten samples from the site. All error bars represent 1 s.e.m. (d) Dose response curve obtained from representative samples with K-Feldspar $pIRIR_{200,290}$ protocol. Lx/Tx represents the sensitivity-corrected luminescence intensity to the test dose.

Zone 4 is indicative of a typical steppe-grassland ecosystem that is now widely distributed from the central Chinese Loess Plateau to southern Mongolia. *Artemisia* was probably the dominant genus, although it is typically over-represented in pollen diagrams. Because its species diversity is very low, we conclude *Artemisia* pollen represents a relatively arid steppe environment. If we consider changes in vegetation zones on the Chinese Loess Plateau during glacial and interglacial periods (Zhou et al., 2014), it can be inferred that an arid steppe-grassland environment was in place during glacial episodes.

Pollen Assemblage Zone 3
*(*Pinus-Syringa-Artemisia-*Chenopodiaceae) (15.2–14.4 m)*
Representation of trees such as *Pinus* and *Betula* increases significantly, and other arboreal pollen types appear (e.g., *Ulmus*, *Quercus*, *Syringa*, and *Hippophae*). Herbaceous pollen decreases from Zone 5 to this zone and *Artemisia* deceases from 80% to ~20% of the assemblage. There are also significant changes in herbaceous taxa present, including members of the Gramineae (Poaceae), Asteraceae, Cyperaceae, and Ranunculaceae families and the genus *Humulus*.

Zone 3 is indicative of an open wooded-grassland that is now distributed in river valleys and semi-humid regions in the area. An increase in the proportion of arboreal pollen and herbaceous pollen diversity reflects the expansion of woodland and humid grassland ecotypes and shrinking steppe-grassland vegetation. Concomitantly, the increase in *Typha* and pollen of members of the Cyperaceae family suggests an expansion of wetlands in the region. This may be related to alterations in local topography and hydrological regime, but, more likely, to changes in global climate. Overall, Pollen Assemblage Zone 3 reflects a wooded-grassland vegetation community with some wetland niches also present; this configuration is also an indicator of the relative wetness of the climate.

Pollen Assemblage Zone 2
*(*Pinus-Poaceae-Artemisia-*Chenopodiaceae) (14.4–13.2 m)*
Zone 3 is similar to Zone 4 in that it reflects an open wooded-grassland, but arboreal pollen is more abundant in Zone 2. Arboreal pollen frequencies reach relatively low levels. *Pinus*, *Syringa*, and *Ulmus* frequencies decrease, however *Betula* pollen increases. Members of the Gramineae (Poaceae) and

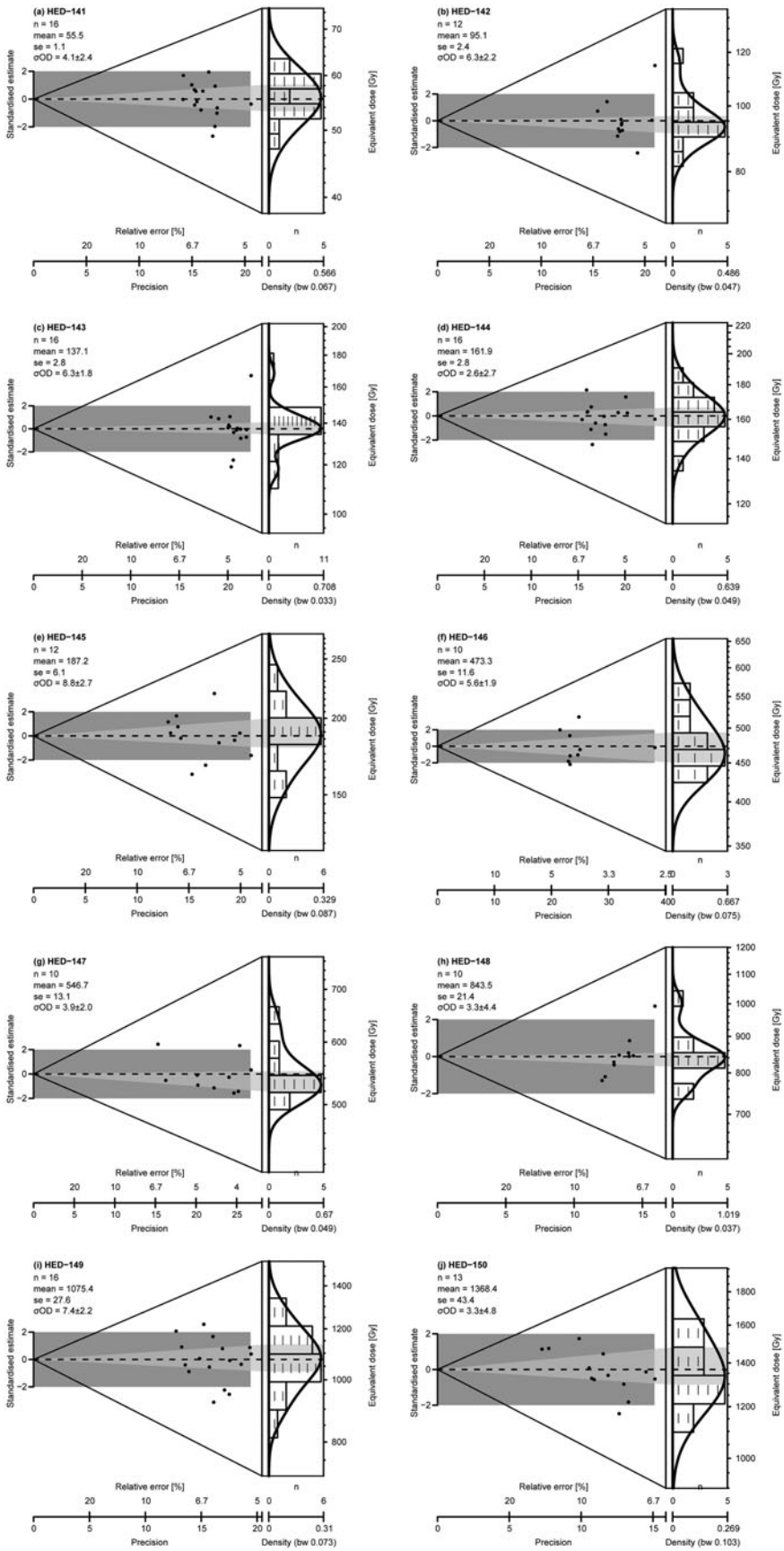

Figure 6. Equivalent dose distributions of all samples.

Table 2. Quartz OSL and K-feldspar pIRIR290 dating results for the Dayao section. The absolute uncertainty of water content is ± 5%; (n) denotes the number of aliquots contributing to the D_e calculation ("Qz" = quartz and "KF" = K-feldspar).

Sample	Depth (m)	Mineral	Wt% (%)	U (ppm)	Th (ppm)	K (%)	D_e (Gy)	Dose rate (Gy/ka)	n	Age (ka)	σOD (%))
HED-141	0.5	Qz	12.67	2.01 ± 0.08	10.3 ± 0.3	1.74 ± 0.06	55.5 ± 1.1	2.81 ± 0.11	16	19.7 ± 0.9	4.1 ± 2.4
HED-142	2.0	Qz	11.78	2.10 ± 0.09	10.1 ± 0.3	1.79 ± 0.06	95.1 ± 2.4	2.83 ± 0.12	12	33.7 ± 1.4	6.3 ± 2.2
HED-143	3.6	Qz	12.65	2.48 ± 0.10	12.1 ± 0.3	1.78 ± 0.06	137.1 ± 2.8	2.96 ± 0.12	16	46.3 ± 2.1	6.3 ± 1.8
HED-144	4.5	Qz	10.83	2.18 ± 0.09	10.7 ± 0.3	1.83 ± 0.06	161.9 ± 2.8	2.90 ± 0.12	16	55.9 ± 2.5	2.6 ± 2.7
HED-145	5.0	Qz	12.14	2.16 ± 0.09	11.2 ± 0.3	1.85 ± 0.06	187.2 ± 6.1	2.90 ± 0.12	12	64.7 ± 3.4	8.8 ± 2.7
HED-146	6.6	KF	9.59	1.94 ± 0.09	11.3 ± 0.3	1.91 ± 0.06	473 ± 12	3.77 ± 0.19	10	126 ± 7	5.6 ± 1.9
HED-147	8.3	KF	10.09	2.05 ± 0.10	12.9 ± 0.6	1.68 ± 0.08	547 ± 13	3.72 ± 0.19	10	147 ± 8	3.9 ± 2.0
HED-148	9.3	KF	10.26	2.13 ± 0.09	12.7 ± 0.4	2.05 ± 0.06	843 ± 21	4.01 ± 0.20	10	210 ± 12	3.3 ± 4.4
HED-149	11.1	KF	9.87	2.11 ± 0.09	12.3 ± 0.3	2.28 ± 0.06	1075 ± 28	4.18 ± 0.21	16	257 ± 14	7.4 ± 2.2
HED-150	13.5	KF	16.82	1.86 ± 0.09	12.7 ± 0.4	2.44 ± 0.07	>1368 ± 43	4.01 ± 0.19	13	>341 ± 20	3.3 ± 4.8

Chenopodiaceae families increase, together with herbaceous taxa. The increase in pollen proportions of members of the Gramineae (Poaceae) and Chenopodiaceae families and the decrease in arboreal pollen reflect an expansion of steppe-grassland vegetation and the shrinking of woodland niches, perhaps indicating a degree of cooling and drought during this period.

Pollen Assemblage Zone 1 (Chenopodiaceae-Artemisia-Pinus*) (13.2–10.8 m)*

Here, arboreal pollen increases on average, including all tree types except *Betula* (e.g., *Syringa* and *Hippophae*), which seems to have decreased. Taxa of the Gramineae (Poaceae) decreased significantly, but *Humulus* and members of the Cyperaceae and Ranunculaceae families, along with taxonomic diversity in general, increased. This zone reflects an increase in woodland and wetland ecosystems and a typical wooded-grassland covering the region. This increase in arboreal vegetation and decrease in steppe-grassland taxa probably resulted from increased summer precipitation.

Annual temperature and precipitation values reconstructed from fossil pollen data for the Dayao sequence reflect clear variations corresponding to field-defined lithological changes (Fig. 9), with higher average annual precipitation and temperature values in the gravel and sand layers and lower average values in the sandy silt and silt layers. As shown in Figure 7, both annual precipitation and temperature display at least two cyclical changes, with the average precipitation and temperature values for these four cyclical periods corresponding to those pollen assemblage zones, are 6.7 ± 0.8°C/585 ± 20 mm, 1.5 ± 1.5°C/396 ± 60 mm, 10.1 ± 1.1°C/786 ± 58 mm, and 3.8 ± 0.4°C/270 ± 26 mm, respectively. Through correlation with stacked magnetic susceptibility records (χ_{fd}) and the marine oxygen isotope sequence ($\delta^{18}O$) representing the East Asian summer monsoon and global temperature changes, respectively, we interpret two peaks between 12.0 m and 13.2 m and between 14.2 m and 15.4 m deep as MIS 9 and MIS 11 according to OSL dating results. According to micromorphological and geochemical studies of the fourth paleosol layer (S4) in Shaanxi conducted by Dong et al. (2010), it is estimated that the mean annual precipitation and temperature there during MIS 11 are similar to those in Nanjing in central China at present, with values ~450 mm and 4°C higher than at present. Their conclusion also agrees with that of Guo et al. (1998), who suggested that the S4 paleosol was formed under subtropical semi-humid climate conditions with a tentatively estimated mean annual temperature of at least 4–6°C greater and a mean annual precipitation of 200–300 mm higher than the present-day. In addition, the semi-quantitative estimation of paleo-precipitation based on magnetic susceptibility suggests an annual precipitation value of 600–700 mm during MIS 11 (Maher et al., 1994; Hao and Guo, 2005; Song et al., 2014). These studies support our quantitative MAT reconstruction results, which indicate that the mean annual precipitation and temperature values in the Dayao area during MIS 11 were ~300 mm and 4°C higher than today.

DISCUSSION AND CONCLUSIONS

Chronology of the Dayao archaeological site and estimation of the age of human occupation

The Dayao archaeological site is located in Inner Mongolia, which is a transitional zone between the great Eurasian steppe-grasslands and the North China Plain. As a result, this site may yield critical information relating to Pleistocene East-West cultural exchanges, as demonstrated by recent finds from the Jinsitai Cave site (Li et al., 2018), which contains a Middle Paleolithic Mousterian

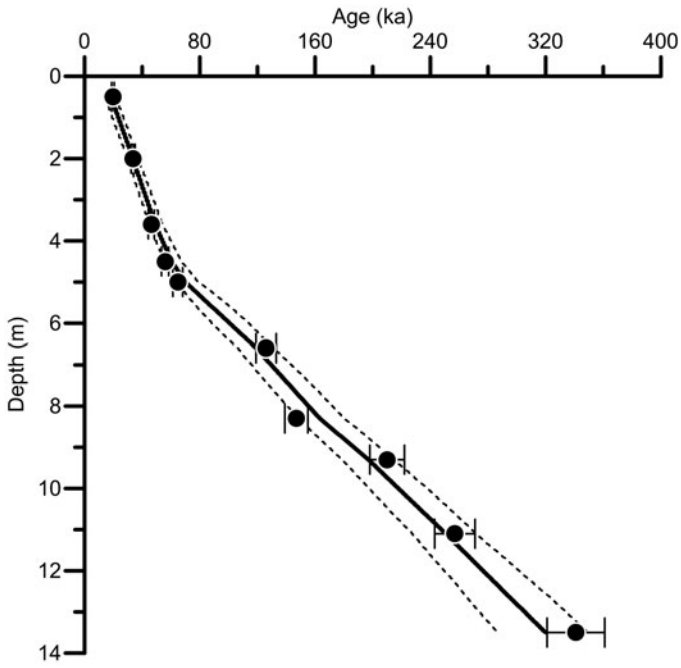

Figure 7. The age-depth correlation of the Dayao section, which is modeled using Bayesian statistics. The solid cycles correspond to the OSL ages. Dashed lines and solid lines indicate 95% confidence intervals and the single best model based on the mean age for each depth, respectively.

assemblage, including Levallois technology, similar to those found farther west. As a representative early Paleolithic site located in currently arid North China, Dayao may also generate evidence of human adaptation to changing environments during the Pleistocene. When the site was discovered in the last century, it immediately attracted the attention of many archaeologists and Quaternary geologists (Wang and Olsen, 1985). During the first series of excavations conducted there in the 1980s, vertebrate faunal remains were discovered, including those of *Megaloceros pachyosteus*, *Equus sanmeniensis*, Rhinocerotinae, *Struthio* sp., *Allactaga sibirica*, *Ochotona daurica*, *Dipus sagitta*, *Microtus brandtoides*, *Cricetulus* cf. *C. griseus*, and *Citellus* cf. *C. mongolicus* (Wang and Olsen, 1985; Wang, 2002). This faunal assemblage is similar to that of some Chinese middle Pleistocene sites, including the *Homo erectus* occupation at Zhoukoudian Locality 1, near Beijing (Chen et al., 1996; Cheng et al., 1997) and Jinniushan, Liaoning (Team, 1976), possibly suggesting an early to middle Pleistocene age for the Dayao site. Detailed thermoluminescence (TL) dating and paleomagnetic studies have been carried out at Dayao, generating wildly different ages. For example, TL determinations made on two samples of burned soil collected in proximity to a *Megaloceros pachyosteus* fossil at ~13.0 m depth generated two dissimilar ages of 113 ± 10 ka and 315 ± 28 ka (Wang, 2002). However, paleomagnetic measurements revealed that the Matuyama/Brunhes boundary was detectable at about 13.4 m, and two magnetic excursions were also identified ~3.5 m and 6.5 m deep (Wang, 2002), correlated with the Laschamp and Blake events, respectively, indicating an age range minimally spanning from 780–20 ka.

Reliability of the luminescence ages are evaluated in the following ways. First, the recycling ratios of the aliquots used for D_e determination are all within an acceptable range (0.9–1.1), for which the recuperation is <5%, suggesting that D_e values yielded using the SAR and $pIRIR_{200,290}$ protocols are reliable. Second, the ages are all within the upper dating range, which was assessed by comparison between the D_e and $2D_0$ values. The quartz OSL signal for the upper four samples are not as saturated since the D_e values are generally smaller than the corresponding $2D_0$ value of ~160 Gy. Although quartz OSL dating is not applicable to the lower samples due to signal saturation, the pIRIR290 signal is proven to be unsaturated, as determined by a D_0 value of ~700 Gy. The lowermost sample is likely close to saturation, for which a minimum age was determined. Third, signal bleaching seems not to be a problem for the samples dated, as suggested by the following reasons: (1) aeolian origin of the fine components of sediments in the Dayao site; and (2) although the pIRIR290 signal is bleached slower than the corresponding quartz OSL signal and the pIRIR signals with lower stimulation temperatures, the residual dose deriving from potential partial bleaching is not problematic for the relatively old ages in this study.

The magnetostratigraphic results presented here demonstrate that most of the samples analyzed reflect normal polarity. Only two samples from 7.8 m to 8.5 m in depth show transitional magnetic behavior possibly attributable to bioturbation, suggesting that the basal age of the Dayao sequence is younger than 780 ka—magnetostratigraphic results quite different from those previously reported by Wang (2002). Because no geomagnetic polarity transition event has been detected, further paleomagnetic age constraints are needed.

The Quaternary loess-paleosol sequences of the Chinese Loess Plateau have long been regarded as near-continuous records of the East Asian monsoon regime (Kukla and An, 1989; Liu and Ding, 1998; Ding et al., 2002). Alternating soil and loess deposits are commonly interpreted as an indication of the waxing and waning of East Asian monsoon circulation, with soil-forming periods corresponding to a strengthened summer monsoon and loess deposits to a more intense winter monsoon in response to glacial and interglacial climate changes (An et al., 1990; Guo et al., 1998). Loess-paleosol sedimentary sequences, therefore, provide a reliable record for stratigraphic and paleoclimatic correlations over large areas. The presence of the last glacial Malan Loess (L1) capping the Dayao section, as indicated by the OSL ages ranging from 64.7 ± 3.4 ka to 19.7 ± 0.9 ka yielded by samples from the upper 5 m, leads us to conclude that the two paleosol

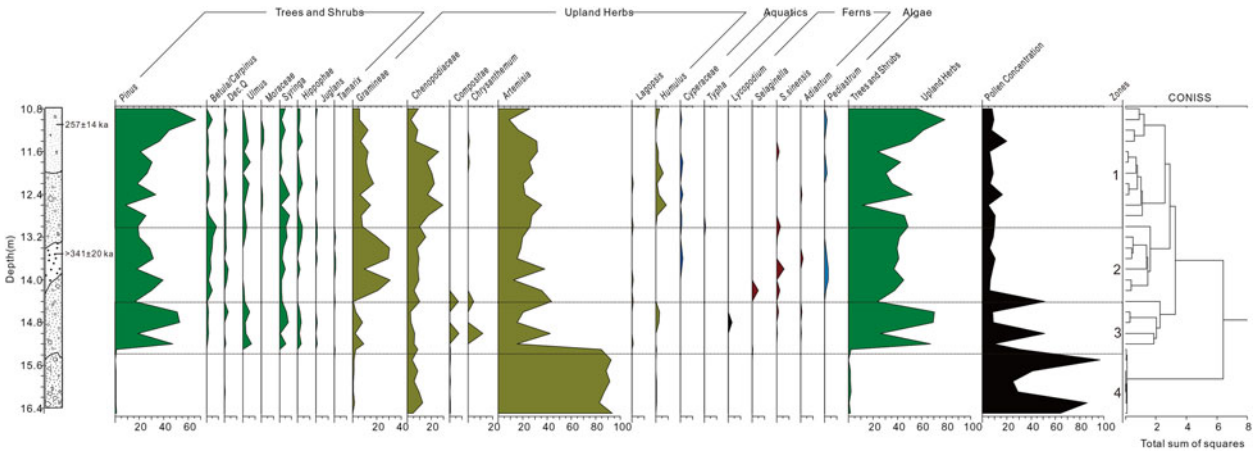

Figure 8. (color online) Percentage diagram of major pollen taxa from the Dayao site.

layers detectable in the upper and middle units of this sedimentary sequence can be correlated with the first (S1) and second (S2) pedocomplexes found in typical Chinese Loess Plateau Quaternary loess sequences without any significant hiatuses, which were deposited during Marine Isotope Stages (MIS) 5 and 7, respectively. Our OSL dating results demonstrate that the Dayao site samples recovered from 4.5 m and 6.6 m deep, which are located near the top of and in the lower portion of the paleosol layer, respectively, yield a bracketing age range of 126 ± 7 ka to 64.9 ± 3.4 ka, confirming that this layer corresponds with MIS 5. The OSL sample taken 9.3 m deep in the sequence from the middle of the second paleosol layer generated an age of 210 ± 12 ka, corresponding with MIS 7, providing further support for our hypothesis that the loess-paleosol sequence visible in the upper and middle units of the Dayao section is continuous.

Paleoclimatic data (Fig. 9, annual temperature and precipitation values), palynologically generated for the gravel- and sand-dominated sediments in the lower unit at Dayao, indicate at least two warm/wet-cold/dry cycles corresponding to glacial-interglacial climate changes. In the absence of significant long-term sedimentary hiatuses during deposition from the middle unit upward, these two climatic cycles can be correlated with the period from MIS 9 to MIS 12. To provide further age constraints on climate-stratigraphic correspondence with the $\delta^{18}O$-based global climate change record and other proxy measures, two OSL samples were collected at 11.1 m depth (HED-149), ~70 cm above the lower unit, and 13.5 m deep (HED-150) in interbedded silt layers in the middle unit. As shown in the integrative dose response curve of the two samples fitted with single saturating exponential functions, all aliquots of sample HED-149 generated dose values smaller than $2\times D_0$ values (1450 ± 70 Gy), indicating that they are capable of measuring the dose of interest and can be reliably used for age estimation. The OSL age derived for sample HED-149 was 257 ± 14 ka, suggesting that the pale silt layer below the second paleosol stratum corresponds with MIS 8. For sample HED-150, however, the feldspar post-IR IRSL signal was nearly saturated with dose values approximating or, occasionally, slightly exceeding the $2\times D_0$ values. Therefore, the age of this sample, calculated by the mean dose of these aliquots, is possibly underestimated somewhat and only represents the *terminus ante quem* of the sample. In spite of the potential age underestimation of this sample, it can still provide partial age constraint for our correlation. In fact, ca. 341 ± 20 ka falls within MIS 10, which is in accordance with our hypothesis that these silt layers developed during a cold glacial period, and indicates that there are no significant sedimentary hiatuses present. Thus, we conclude that the other detectable climate change cycle occurred earlier, below the silt layers, corresponding with MIS 12 and MIS 11.

The artifact occurrence at the Dayao site has an early date; ca. 430 ka, as suggested by the start date of MIS 11 (Lisiecki and Raymo, 2005), and constitutes the earliest and the northernmost archaeological record yet reported in arid northwest China. The intermittent occurrence of multiple artifact-bearing layers in the sediment sequence at Dayao indicates that this site was repeatedly occupied by hominins beginning ca. 430 ka. During the past few decades, archaeological investigations in this area have revealed other Paleolithic sites near Dayao, including Dayao Locality 2 (Xu et al., 2013), Locality 8, and the 27th Cave (Wang et al., 2014), among others, most of which are associated with the Late Paleolithic, suggesting long-term human occupation in this region. However, preliminary archaeological studies at these sites indicate that artifacts produced in the early period of their occupation are dominated by roughly modified chunks and debris, and a low proportion of flaked products (e.g., flakes and blades) for the fabrication of formal tools. Tools are mostly characterized by little, if any, use wear, indicating that hominins obtained lithic raw material *in situ*, using Dayao as a convenient quarry-workshop for producing artifacts taken off-site to exploit the surrounding arid environment.

Implications for human migration and dispersal into arid northwest China during glacial-interglacial periods

The extensive mid-latitude arid belt dominated by deserts extending from the Atlantic coast of North Africa, through the Middle East, and deep into eastern Asia comprises one of the most fundamental environmental and biogeographical features in the world, which may have profoundly affected the course of human evolution and the nature of human settlement in those areas. For example, the Sahara-Arabian arid and semi-arid zone separating the African and Eurasian continents has long acted as a geographical filter and launch zone for migrations and dispersals of *H. sapiens* out of Africa (Osborne et al., 2008; Castañeda et al., 2009; Drake et al., 2011). On the one hand, this desert zone comprised the most significant barrier to the

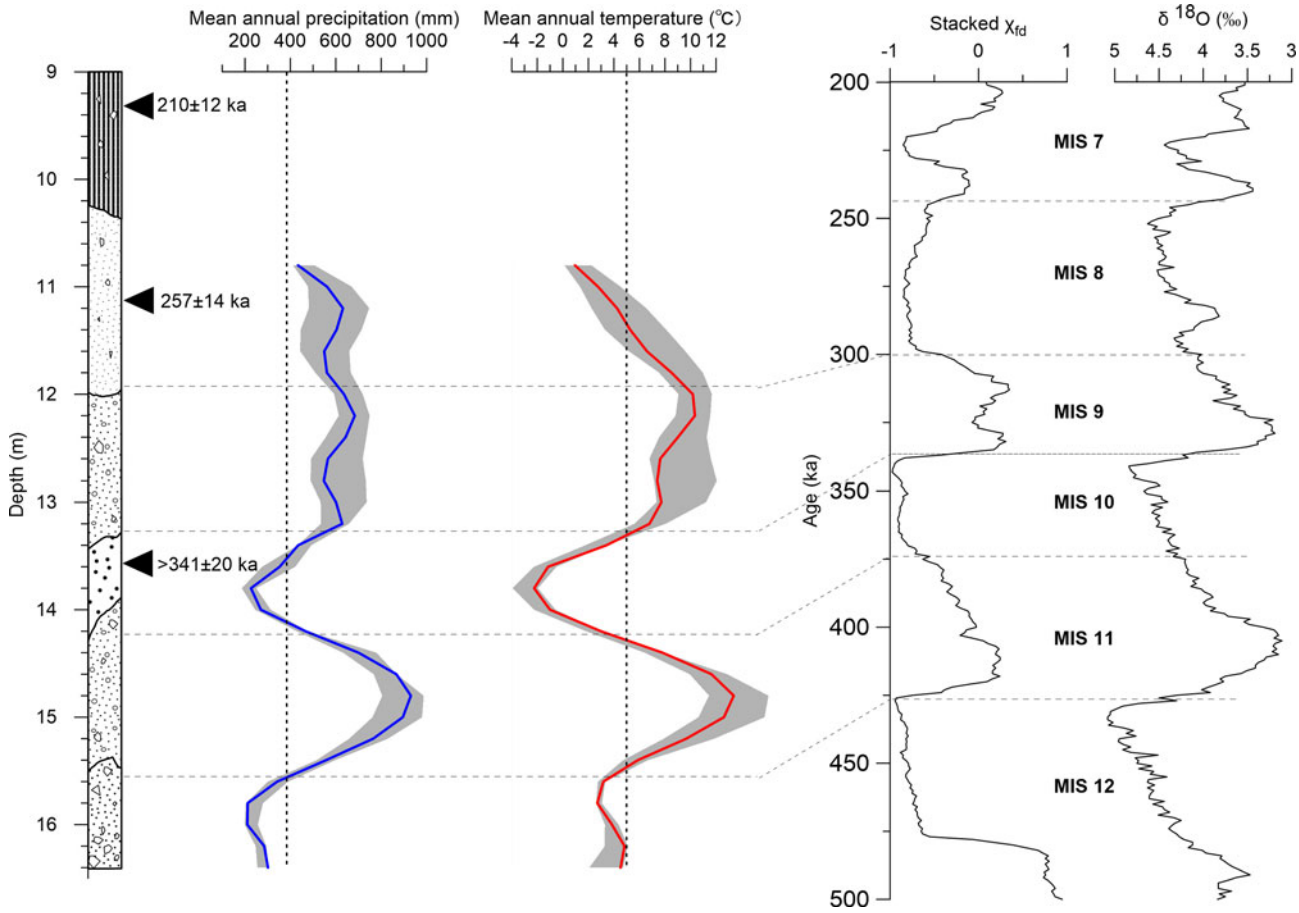

Figure 9. (color online) Variations in annual precipitation and temperature quantitatively reconstructed from pollen analysis and stratigraphic correlation, stacked χ_{fd} in the Chinese loess-soil sequence (Hao et al., 2012) and marine $\delta^{18}O$ records (Lisiecki et al., 2005). The vertical dashed lines indicate the present-day values of the annual average precipitation and annual average temperature at the Dayao site.

movement of hominins northward into southwest Asia and Europe, and, on the other hand, likely played a motivating role in processes of colonization by providing a salubrious corridor for human migration during relatively wet climatic periods (Castañeda et al., 2009). Some authors even propose that this mid-latitude arid belt was an optimal region for Pleistocene hominin occupation—a crucible of human evolution and central to Pleistocene hominin expansions rather than merely a corridor that was rapidly traversed and left behind (Finlayson, 2013).

In continental Eurasia, vast semi-arid drylands may have offered a desirable landscape for the earliest contacts between anatomically modern humans and Neanderthals, including interbreeding (Green et al., 2010). Given the selective advantages of anatomically modern *H. sapiens* for long-term survival and settlement in Asia owing to enhanced physical and, possibly, technological adaptations to arid environments, they ultimately replaced Neanderthals, successfully settling most niches on the continent (Dennell, 2013a). The increasing mid-Pleistocene aridification of much of continental Asia would have impeded human immigration across the continent and possibly led to the isolation of *H. erectus* in China from their counterparts in Central Asia and the West (Dennell, 2013b), due to the local scarcity of critical resources for survival, such as potable water and edibles derived from plants and animals. Dennell (2013b) has persuasively argued that any meaningful adaptation of *H. sapiens* to true desert environments occurred only in the Holocene or, perhaps, the terminal Pleistocene, which is a perspective shared by a number of other scholars (Barker and Gilbertson, 2003; Veth et al., 2008).

Virtually all known middle Pleistocene archaeological and human paleontological sites in China are located on or near the North China Plain, in central China, and in eastern coastal areas of the country in relatively moist environments, but with distinct seasonal variations (e.g., Zhoukoudian, Nihewan, Miaohoushan, Lantian, and Nanjing, among many others) (Fig. 10a, b). Thus, the occurrence of artifacts in the Dayao site at ca. 430 ka may indicate that earlier Paleolithic populations attempted to enter China's vast dry northwest to exploit new resources and territories. Alternatively, drylands may have been simply used as convenient sources of exposed lithic raw material at that time, representing human range expansion into familiar habitats during humid periods rather than an adaptation to arid conditions as such (Foley et al., 2013). Certainly, it is true that China's arid northwest was not extensively inhabited by people and their complex cultural adaptations until the late Pleistocene or even the Holocene (Fig. 10c).

River valleys and chains of perennial lakes in drylands potentially created viable migration pathways or "green corridors" (Osborne et al., 2008; Coulthard et al., 2013) and "mega lake corridors" (Pachur and Rottinger, 1997). In North Africa and the Arabian Peninsula, such relatively lush strips formed during warm and wet phases in the late middle Pleistocene and late Pleistocene, providing the opportunity for anatomically modern

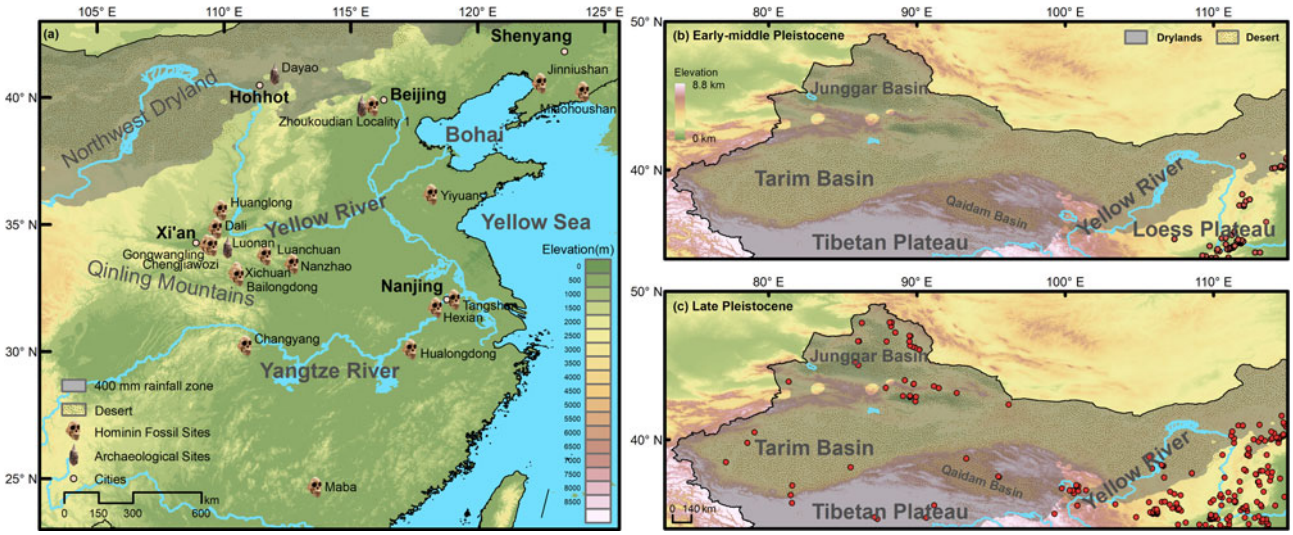

Figure 10. (color online) Representative early–middle Pleistocene human fossils and Paleolithic sites in China (a) and distribution of Paleolithic sites in and around the northwest Chinese drylands during the early–middle Pleistocene (b) and late Pleistocene (c), respectively.

humans to move out of Africa and disperse into Eurasia, as is suggested by archaeological remains and fossils of *H. sapiens* associated with buried paleo-river channels in the region (Osborne et al., 2008; Petraglia et al., 2011; Breeze et al., 2016). The Huanghe (Yellow River) in North China, originating on the northeastern Tibetan Plateau, may also have acted as a corridor for hominin dispersal from Inner Mongolia to the northeast Tibetan Plateau, where game and other resources were more abundant. At present, much of this corridor is densely inhabited in ever-expanding urban centers. However, some Pleistocene age archaeological sites situated in this corridor, such as the Shuidonggou localities near Yinchuan, Ningxia (Li et al., 2013; Madsen et al., 2001), evince deeper human penetration into dryland ecosystems. During the middle Pleistocene, because of synchronous strengthened aridification of northwest China and the expansion of deserts in Central Asia, as reflected by the marked increase in eolian dust deposition (Ding et al., 2002), it has been suggested that impediments to the northward dispersal of North Chinese hominins into Central Asia would have become much greater after ca. 500 ka (Dennell, 2013b). Therefore, movement along the course of the Yellow River into the arid northwest became a logical migration route. The Paleolithic remains at Dayao predating ca. 400 ka may record an initial human attempt to enter and exploit China's vast, dry northwest via this Yellow River corridor.

However, riverine corridors may not always have been viable due to Pleistocene environmental changes, especially during full glacial and interglacial periods (Osborne et al., 2008; Cunningham and Wallinga, 2010; Breeze et al., 2016). As is recorded in Quaternary loess-paleosol sequences, the topographic boundaries of deserts in North China were not fixed, but expanded and contracted periodically as the East Asian monsoon fluctuated in response to alternating glacial and interglacial conditions. During relatively moist interglacial periods, the northern front of the summer monsoon regime moved north into regions currently occupied by deserts. The retreat of the summer monsoon precipitation belt during relatively cold and dry glacial episodes triggered intensified environmental desiccation, causing the significant southward extension of desert conditions. According to previous studies (Hao and Guo, 2005; Yang and Ding, 2008), the maximum northward and southward displacements of the northern front of the summer monsoon regime during the past four interglacial-glacial cycles may have exceeded ~200 and ~500 km, respectively, in comparison to present-day conditions. The repeated expansion and contraction of drylands may have profoundly affected hominin migration through such areas via the Yellow River corridor. First, as the size of desert areas expanded southeastward during glacial periods, the Yellow River at its Great Bend would have been encircled by the Mu Us Desert (Maowusu Shamo), virtually cutting off a potential pathway from the Dayao site to the Yellow River valley, whereas the retreat of the desert boundary would have created a potential entryway to the corridor.

Geological boreholes drilled in the same region provide supporting evidence for our hypothesis, demonstrating that coarse eolian sand layers and silty clay strata of lacustrine origin were laid down alternately during the middle Pleistocene (Chen et al., 2008; Nie, 2019). Second, moister conditions also caused the corridor to be well vegetated, presumably encouraging the availability of critical resources, such as both large and small mammalian game, birds, fish, and edible plants. Conversely, of course, during more arid periods, desert lands expanded, creating circumstances unlikely to have encouraged, or even permitted, hominin dispersals.

In fact, these warm and moist interglacials or interstadials during the middle and late Pleistocene (e.g., MIS 3, 5, 7, 9, 11, 13, 15) have been regarded as "windows of opportunity" for hominins and associated mammalian faunas to disperse into (and perhaps out of) China (Dennell, 2016; Dennell et al., 2020). During the interval between MIS 15 and MIS 11, sediment records from Lake Baikal in southern Siberia reflect predominantly interglacial conditions, with no indication of montane glaciation (Prokopenko et al., 2002); while East Asia was dominated by an extremely strong summer monsoon with the 100–300 km northward displacement of the monsoonal rainfall belt in comparison with the present and a rainfall increase of 200–600 mm (Guo et al., 1998; Hao and Guo, 2005). Hao et al. (2015) suggested that the very long interglacial climate of this period may have facilitated the second major dispersal episode of African hominins into Eurasia. It may

have also provided the opportunity for the opening of the corridor that allowed the Dayao Paleolithic hominins to exploit the northern drylands eastward and the likely immigration into north China of *H. heidelbergensis*, if one accepts Rightmire's classifications of the Dali and Jinniushan hominins (Rightmire, 1998, 2001; Dennell, 2016).

Cumulatively, our results indicate the earliest hominin occupation of the Dayao site occurred before ca. 400 ka BP during a relatively warm and moist interglacial period, with subsequent occupations also occurring mainly in interglacial episodes characterized by mean annual precipitation and temperature values 200–400 mm and 2–4°C, respectively, higher than today. The chronology of the northern advance of the summer monsoon front may thus provide a time window for human migration northwestward into China's arid northwest along a "green corridor," the geographical and environmental parameters of which we are only beginning to understand. When the summer monsoon precipitation belt retreated south during relatively cold glacial intervals, deserts expanded southeast, intensifying aridification in the Hetao (Ordos) Region, effectively closing this corridor to human migration. The fluctuation of the East Asian summer monsoon, responding to global glacial-interglacial climate changes and other influences played a key role in determining the chronology and spatial dynamics of Paleolithic populations in North China, especially in arid areas.

ACKNOWLEDGMENTS. We greatly appreciate the helpful comments and suggestions from the editors and two reviewers, and thank Drs. Keliang Zhao and Yaoliang Liu for their important input and discussions, and Ting Xu, Jiaxu Liu, and Hao Xie for their invaluable assistance in the field.

Financial support. Our research was generously supported by the Strategic Priority Research Program of the Chinese Academy of Sciences (Award No. XDB26000000) and the National Natural Science Foundation of China (Awards Nos. NSFC 41977380, 41672352, and 41888101), as well the State Key Laboratory of Palaeobiology and Stratigraphy (Nanjing Institute of Geology and Palaeontology, CAS) (No.133105). Olsen's participation was supported by the Chinese Academy of Sciences President's International Fellowship Initiative (PIFI) (Award No. 2018VCA0016) and the Je Tsongkhapa Endowment for Central and Inner Asian Archaeology at the University of Arizona.

References

Aitken, M.J., 1985. *Thermoluminescence Dating*. Academic Press, London, Orlando, Montreal.

An, Z.S., Liu, T.S., Lu, Y.C., Porter, S.C., Kukla, G., Wu, X.H., Hua, Y.M., 1990. The long-term paleomonsoon variation recorded by the loess-paleosol sequence in central China. *Quaternary International* **7–8**, 91–95.

Arnold, L.J., Bailey, R.M., Tucker, G.E., 2007. Statistical treatment of fluvial dose distributions from southern Colorado arroyo deposits. *Quaternary Geochronology* **2**, 162–167.

Barker, G., Gilbertson, D., 2003. *The Archaeology of Drylands: Living at the Margin*. Routledge, London, New York.

Bøtter-Jensen, L., Andersen, C.E., Duller, G.A., Murray, A.S., 2003. Developments in radiation, stimulation and observation facilities in luminescence measurements. *Radiation Measurements* **37**, 535–541.

Breeze, P.S., Groucutt, H.S., Drake, N.A., White, T.S., Jennings, R.P., Petraglia, M.D., 2016. Palaeohydrological corridors for hominin dispersals in the Middle East ~250–70,000 years ago. *Quaternary Science Reviews* **144**, 155–185.

Buylaert, J.P., Jain, M., Murray, A.S., Thomsen, K.J., Thiel, C., Sohbati, R., 2012. A robust feldspar luminescence dating method for middle and late Pleistocene sediments. *Boreas* **41**, 435–451.

Buylaert, J.P., Murray, A.S., Huot, S., 2008. Optical dating of an Eemian site in northern Russia using K-feldspar. *Radiation Measurements* **43**, 715–720.

Buylaert, J.P., Vandenberghe, D., Murray, A.S., Huot, S., De Corte, F., Van den Haute, P., 2007. Luminescence dating of old (>70 ka) Chinese loess: a comparison of single-aliquot OSL and IRSL techniques. *Quaternary Geochronology* **2**, 9–14.

Castañeda, I.S., Mulitza, S., Schefuß, E., dos Santos, R.A.L., Damsté, J.S.S., Schouten, S., 2009. Wet phases in the Sahara/Sahel region and human migration patterns in North Africa. *Proceedings of the National Academy of Sciences* **106**, 20159–20163.

Chen, F.H., Fan, Y.X., Madsen, D.B., Chun, X., Zhao, H., Yang, L.P., 2008. Preliminary study on the formation mechanism of the "Jilantai-Hetao" megalake and the lake evolutionary history in Hetao region. *Quaternary Sciences* **28**, 866–873. [in Chinese]

Cheng, J., Tian, M.Z., Cao, B.X., Zhao, Z.Z., 1997. New Quaternary mammalian faunas and cave deposits in the Zhoukoudian area, Beijing. *Acta Geologica Sinica* (*English Edition*) **71**, 231–243.

Chen, J., Tian, M.Z., Cao, B.X., Li, L.Y., 1996. Evolution of Quaternary mammalian assemblages and environmental changes in Zhoukoudian Area, Beijing. *Geoscience-Journal of Graduate School, China University of Geosciences* **10**, 202–212.

Clark, P.U., Archer, D., Pollard, D., Blum, J.D., Rial, J.A., Brovkin, V., Mix, A.C., Pisias, N.G., Roy, M., 2006. The middle Pleistocene transition: characteristics, mechanisms, and implications for long-term changes in atmospheric pCO_2. *Quaternary Science Reviews* **25**, 3150–3184.

Coulthard, T.J., Ramirez, J.A., Barton, N., Rogerson, M., Brücher, T., 2013. Were rivers flowing across the Sahara during the last interglacial? Implications for human migration through Africa. *PloS ONE* **8**, e74834. https://doi.org/10.1371/journal.pone.0074834.

Cunningham, A.C., Wallinga, J., 2010. Selection of integration time intervals for quartz OSL decay curves. *Quaternary Geochronology* **5**, 657–666.

Dennell, R., 2003. Dispersal and colonisation, long and short chronologies: how continuous is the early Pleistocene record for hominids outside East Africa? *Journal of Human Evolution* **45**, 421–440.

Dennell, R., 2013a. Hominins, deserts, and the colonisation and settlement of continental Asia. *Quaternary International* **300**, 13–21.

Dennell, R.W., 2013b. The Nihewan Basin of North China in the early Pleistocene: continuous and flourishing, or discontinuous, infrequent and ephemeral occupation? *Quaternary International* **295**, 223–236.

Dennell, R.W. 2016. Life without the Movius Line. *Quaternary International* **400**, 14–22.

Dennell, R.W., Martinón-Torres, M., Bermudez de Castro, J.M. and Gao X., 2020. A demographic history of late Pleistocene China. *Quaternary International* **559**, 4–13. https://doi.org/10.1016/j.quaint.2020.03.014.

Ding, Z.L., Derbyshire, E., Yang, S.L., Yu, Z.W., Xiong, S.F., Liu, T., 2002. Stacked 2.6-Ma grain size record from the Chinese loess based on five sections and correlation with the deep-sea $\delta^{18}O$ record. *Paleoceanography* **17**, 5–1–5–21.

Dong, H.M., Zhao, J.B., Song, Y.G., 2010. Geochemical components and paleoenvironment implication for S4 paleosol in Shaolingyuan, Chang'an County. *Scientia Geographica Sinica* **30**, 904–909.

Drake, N.A., Blench, R.M., Armitage, S.J., Bristow, C.S., White, K.H., 2011. Ancient watercourses and biogeography of the Sahara explain the peopling of the desert. *Proceedings of the National Academy of Sciences* **108**, 458–462.

Duller, G.A.T., 2008. Single-grain optical dating of Quaternary sediments: why aliquot size matters in luminescence dating. *Boreas* **37**, 589–612.

Durcan, J.A., King, G.E., Duller, G.A.T., 2015. DRAC: dose rate and age calculator for trapped charge dating. *Quaternary Geochronology* **28**, 54–61.

Faegri, K., Iversen, J., 1975. *Textbook of Pollen Analysis*. Blackwell Scientific, Oxford.

Feng, X.W., 2008. *Lithic Industry of the Sidaogou Locality, Dayao, Inner Mongolia*. Ph.D. thesis, Beijing, Chinese Academy of Science, 180 pp.

Fick, S.E., Hijmans, R.J., 2017. WorldClim 2: new 1-km spatial resolution climate surfaces for global land areas. *International Journal of Climatology* **37**, 4302–4315.

Finlayson, C., 2013. The Water Optimisation Hypothesis and the human occupation of the mid-latitude belt in the Pleistocene. *Quaternary International* **300**, 22–31.

Foley, R.A., Maíllo-Fernández, J.M., Lahr, M.M., 2013. The Middle Stone Age of the central Sahara: biogeographical opportunities and technological strategies in later human evolution. *Quaternary International* **300**, 153–170.

Galbraith, R.F., Roberts, R.G., Laslett, G.M., Yoshida, H., Olley, J.M., 1999. Optical dating of single and multiple grains of quartz from Jinmium rock shelter, northern Australia: Part I, experimental design and statistical models. *Archaeometry* **41**, 339–364.

Green, R.E., Krause, J., Briggs, A.W., Maricic, T., Stenzel, U., Kircher, M., Patterson, N., Li, H., Zhai, W., Fritz, M.H.-Y., 2010. A draft sequence of the Neandertal genome. *Science* **328**, 710–722.

Guérin, G., Mercier, N., Adamiec, G., 2011. Dose-rate conversion factors: update. *Ancient TL* **29**, 5–8.

Guiot, J., 1990. Methodology of the last climatic cycle reconstruction in France from pollen data. *Palaeogeography, Palaeoclimatology, Palaeoecology* **80**, 49–69.

Guiot, J., Goeury, C., 1996. PPPBASE, a software for statistical analysis of paleoecological and paleoclimatological data. *Dendrochronologia* **14**, 295–300.

Guo, Z.T., Liu, T.S., Fedoroff, N., Wei, L.Y., Ding, Z.L., Wu, N.Q., Lu, H.Y., Jiang, W.Y., An, Z.S., 1998. Climate extremes in loess of China coupled with the strength of deep-water formation in the North Atlantic. *Global and Planetary Change* **18**, 113–128.

Guo, Z.T., Sun, B., Zhang, Z.S., Peng, S.Z., Xiao, G.Q., Ge, J.Y., Hao, Q.Z., *et al.*, 2008. A major reorganization of Asian climate by the early Miocene. *Climate of the Past* **4**, 153–174.

Hao, Q., Wang, L., Oldfield, F., Guo, Z., 2015. Extra-long interglacial in Northern Hemisphere during MISs 15–13 arising from limited extent of Arctic ice sheets in glacial MIS 14. *Nature Scientific Reports* **5**, 12103. https://doi.org/10.1038/srep12103.

Hao, Q.Z., Guo, Z.T., 2005. Spatial variations of magnetic susceptibility of Chinese loess for the last 600 kyr: implications for monsoon evolution. *Journal of Geophysical Research: Solid Earth* **110**, B12101. https://doi.org/10.1029/2005JB003765.

Hao, Q.Z., Wang, L., Oldfield, F., Peng, S.Z., Qin, L., Song, Y., Xu, B., Qiao, Y.S., Bloemendal, J., Guo, Z.T., 2012. Delayed build-up of Arctic ice sheets during 400,000-year minima in insolation variability. *Nature* **490**, 393–396.

Head, M.J., Pillans, B., Farquhar, S.A., 2008. The early–middle Pleistocene transition: characterization and proposed guide for the defining boundary. *Episodes* **31**, 255–259.

Hublin, J.-J., Roebroeks, W., 2009. Ebb and flow or regional extinctions? On the character of Neandertal occupation of northern environments. *Comptes Rendus Palevol* **8**, 503–509.

Huntley, D.J., Baril, M.R., 1997. The K content of the K-feldspars being measured in optical dating or in thermoluminescence dating. *Ancient TL* **15**, 11–13.

Imbrie, J., Berger, A., Boyle, E.A., Clemens, S.C., Duffy, A., Howard, W.R., Kukla, G., Kutzbach, J., Martinson, D.G., McIntyre, A., 1993. On the structure and origin of major glaciation cycles 2. The 100,000-year cycle. *Paleoceanography* **8**, 699–735.

Jain, M., Murray, A.S., Bøtter-Jensen, L., 2003. Characterisation of blue-light stimulated luminescence components in different quartz samples: implications for dose measurement. *Radiation Measurements* **37**, 441–449.

Jones, C.H., 2002. User-driven integrated software lives: "Paleomag" paleomagnetics analysis on the Macintosh. *Computers & Geosciences* **28**, 1145–1151.

Kirschvink, J.L., 1980. The least-squares line and plane and the analysis of palaeomagnetic data. *Geophysical Journal International* **62**, 699–718.

Kukla, G., An, Z.S., 1989. Loess stratigraphy in central China. *Palaeogeography, Palaeoclimatology, Palaeoecology* **72**, 203–225.

Li, F., Kuhn, S.L., Chen, F.Y., Wang, Y.H., Southon, J., Peng, F., Shan, M.C., Wang, C.X., Ge, J.Y., Wang, X.M., 2018. The easternmost Middle Paleolithic (Mousterian) from Jinsitai Cave, North China. *Journal of Human Evolution* **114**, 76–84.

Li, F., Kuhn, S.L., Gao, X., Chen, F.Y., 2013. Re-examination of the dates of large blade technology in China: a comparison of Shuidonggou Locality 1 and Locality 2. *Journal of Human Evolution* **64**, 161–168.

Lisiecki, L.E., Raymo, M.E., 2005. A Pliocene–Pleistocene stack of 57 globally distributed benthic $\delta^{18}O$ records. *Paleoceanography* **20**, PA1003. https://doi.org/10.1029/2004PA001071.

Liu, T.S., Ding, Z.L., 1998. Chinese loess and the paleomonsoon. *Annual Review of Earth and Planetary Sciences* **26**, 111–145.

Madsen, D.B., Li, J.Z., Brantingham, P.J., Gao, X., Elston, R.G., Bettinger, R.L., 2001. Dating Shuidonggou and the Upper Palaeolithic blade industry in North China. *Antiquity* **75**, 706–716.

Maher, B.A., Thompson, R., Zhou, L.P., 1994. Spatial and temporal reconstructions of changes in the Asian palaeomonsoon: a new mineral magnetic approach. *Earth and Planetary Science Letters* **125**, 461–471.

Members of China Quaternary Pollen Data Base (MCQPD), 2000. Pollen-based biome reconstruction at middle Holocene (6 ka BP) and Last Glacial Maximum (18 ka BP) in China. *Acta Botanica Sinica* **42**, 1201–1209. [in Chinese with English Abstract]

Moore, P.D., Webb, J.A., Collison, M.E., 1991. *Pollen Analysis*. Blackwell Scientific, Oxford.

Mu, H.S., Xu, Q.H., Zhang, S.R., Hun, L.Y., Li, M.Y., Li, Y., Hu, Y.N., Xie, F., 2015. Pollen-based quantitative reconstruction of the paleoclimate during the formation process of Houjiayao Relic Site in Nihewan Basin of China. *Quaternary International* **374**, 76–84.

Murray, A.S., Wintle, A.G., 2000. Luminescence dating of quartz using an improved single-aliquot regenerative-dose protocol. *Radiation Measurements* **32**, 57–73.

Murray, A.S., Wintle, A.G., 2003. The single aliquot regenerative dose protocol: potential for improvements in reliability. *Radiation Measurements* **37**, 377–381.

Nie, Z.S., 2019. Stratigraphic division of the upper Pleistocene, environmental change and formation of the Yellow River in the Hetao Basin, Inner Mongolia. *Earth Science Frontiers* **26**, 259–272.

Olley, J.M., Caitcheon, G.G., Roberts, R.G., 1999. The origin of dose distributions in fluvial sediments, and the prospect of dating single grains from fluvial deposits using optically stimulated luminescence. *Radiation Measurements* **30**, 207–217.

Olley, J.M., Pietsch, T., Roberts, R.G., 2004. Optical dating of Holocene sediments from a variety of geomorphic settings using single grains of quartz. *Geomorphology* **60**, 337–358.

Osborne, A.H., Vance, D., Rohling, E.J., Barton, N., Rogerson, M., Fello, N., 2008. A humid corridor across the Sahara for the migration of early modern humans out of Africa 120,000 years ago. *Proceedings of the National Academy of Sciences* **105**, 16444–16447.

Overpeck, J.T., Webb, T., Prentice, I.C., 1985. Quantitative interpretation of fossil pollen spectra: dissimilarity coefficients and the method of modern analogs. *Quaternary Research* **23**, 87–108.

Pachur, H.J., Rottinger, F., 1997. Evidence for a large extended paleolake in the Eastern Sahara as revealed by spaceborne radar lab images. *Remote Sensing of the Environment* **61**, 437–440.

Petraglia, M.D., Alsharekh, A.M., Crassard, R., Drake, N.A., Groucutt, H., Parker, A.G., Roberts, R.G., 2011. Middle Paleolithic occupation on a Marine Isotope Stage 5 lakeshore in the Nefud Desert, Saudi Arabia. *Quaternary Science Reviews* **30**, 1555–1559.

Porter, S.C., 2001. Chinese loess record of monsoon climate during the last glacial–interglacial cycle. *Earth-Science Reviews* **54**, 115–128.

Prentice, I.C., Guiot, J., Huntley, B., Jolly, D., Cheddadi, R. 1996. Reconstructing biomes from palaeoecological data: a general method and its application to European pollen data at 0 and 6 ka. *Climate Dynamics* **12**, 185–194.

Prescott, J.R., Hutton, J.T., 1994. Cosmic ray contributions to dose rates for luminescence and ESR dating: large depths and long-term time variations. *Radiation Measurements* **23**, 497–500.

Prokopenko, A., Williams, D., Kuzmin, M., Karabanov, E.B., Khursevich, G.K., Peck, J.A., 2002. Muted climate variations in continental Siberia during the mid-Pleistocene epoch. *Nature* **418**, 65–68.

Rees-Jones, J., 1995. Optical dating of young sediments using fine-grain quartz. *Ancient TL* **13**, 9–14.

Rightmire, G.P., 1998. Human evolution in the middle Pleistocene: the role of *Homo heidelbergensis*. *Evolutionary Anthropology* **6**, 218–227.

Rightmire, G.P., 2001. Comparison of middle Pleistocene hominids from Africa and Asia. In: Barham, L., Robson-Brown, K. (Eds.), *Human Roots: Africa and Asia in the Middle Pleistocene*. Western Academic and Specialist Press Ltd., Bristol, pp. 123–133.

Roberts, H.M., 2006. Optical dating of coarse-silt sized quartz from loess: evaluation of equivalent dose determinations and SAR procedural checks. *Radiation Measurements* **41**, 923–929.

Shen, G.J., Gao, X., Gao, B., Granger, D.E., 2009. Age of Zhoukoudian *Homo erectus* determined with $^{26}Al/^{10}Be$ burial dating. *Nature* **458**, 198–200.

Smith, B.W., Rhodes, E.J., 1994. Charge movements in quartz and their relevance to optical dating. *Radiation Measurements* **23**, 329–333.

Song, Y., Hao, Q.Z., Ge, J.Y., Zhao, D.a., Zhang, Y., Li, Q., Zuo, X.X., Lü, Y.W., Wang, P., 2014. Quantitative relationships between magnetic enhancement of modern soils and climatic variables over the Chinese Loess Plateau. *Quaternary International* **334–335**, 119–131.

Stevens, T., Buylaert, J.P., Thiel, C., Újvári, G., Yi, S., Murray, A.S., Frechen, M., Lu, H.Y., 2018. Ice-volume-forced erosion of the Chinese Loess Plateau global Quaternary stratotype site. *Nature Communications* **9**, 1–12.

Stewart, J.R., Stringer, C.B., 2012. Human evolution out of Africa: the role of refugia and climate change. *Science* **335**, 1317–1321.

Sun, X.F., Lu, H.Y., Wang, S.J., Yi, L., Li, Y.X., Bahain, J.J., Voinchet, P., Hu, X.Z., Zeng, L., Zhang, W.C., 2017. Early human settlements in the southern Qinling Mountains, central China. *Quaternary Science Reviews* **164**, 168–186.

Team, J.E., 1976. Quaternary mammalian fauna from Jinniushan, Yingkou of Liaoning Province. *Vertebrata PalAsiatica* **14**, 120–127. [in Chinese]

Thomas, D.S.G., 2011. *Arid Zone Geomorphology: Process, Form and Change in Drylands, Third Edition*. John Wiley & Sons, Chichester.

Veth, P., Smith, M., Hiscock, P., 2008. *Desert Peoples: Archaeological Perspectives*. John Wiley & Sons, Oxford.

Wang, F.X., Qian, N.F., Zhang, Y.L., Yang, H.Q., 1997. *Pollen Flora of China, Second Edition*. Science Press, Beijing. [in Chinese]

Wang, Y.H., 2002. Geochronological dating and cultural staging of the site of the Dayao Locality 4 site. *Inner Mongolia Cultural Relics and Archaeology* (*Steppe Cultural Relics*) 6–11. [in Chinese]

Wang, Y.H., Liu, J.X., Shan, M.C., Li, F., Chen, F.Y., 2014. A preliminary report of the stone artifacts from the 27th cave of the Dayao Site. *Acta Anthropologica Sinica* **33**, 51–59.

Wang, Y.P., Olsen, J.W., 1985. Aspects of the Inner Mongolian Palaeolithic. In: Wu, R.K., Olsen, J.W. (Eds.), *Palaeoanthropology and Palaeolithic Archaeology in the People's Republic of China*. Academic Press, New York, London, pp. 243–258.

Wintle, A.G., Murray, A.S., 2006. A review of quartz optically stimulated luminescence characteristics and their relevance in single-aliquot regeneration dating protocols. *Radiation Measurements* **41**, 369–391.

Xi, Y.Z., Ning, J.C., 1994. Study on pollen morphology of plants from dry and semidry areas in China. *Yushania* **11**, 119–191.

Xu, T., Chen, F.Y., Wang, Y.H., 2013. An analysis of the cores and their flaking technology of the Erdaogou Locality of Dayao Site. *Acta Anthropologica Sinica* **32**, 441–453.

Yang, S.L., Ding, Z.L., 2008. Advance-retreat history of the East-Asian summer monsoon rainfall belt over northern China during the last two glacial-interglacial cycles. *Earth and Planetary Science Letters* **274**, 499–510.

Yi, S.W., Buylaert, J.P., Murray, A.S., Lu, H.Y., Thiel, C., Zeng, L., 2016. A detailed post-IR IRSL dating study of the Niuyangzigou loess site in northeastern China. *Boreas* **45**, 644–657.

Zheng, Z., Wei, J.H., Huang, K.Y., Xu, Q.H., Lu, H.Y., Tarasov, P., Luo, C.X., Beaudouin, C., Deng, Y., Pan, A.D., 2014. East Asian pollen database: modern pollen distribution and its quantitative relationship with vegetation and climate. *Journal of Biogeography* **41**, 1819–1832.

Zhou, X.Y., Li, X.Q., Dodson, J., Yang, S.L., Long, H., Zhao, K.L., Sun, N., Yang, Q., Liu, H.B., Zhao, C., 2014. Zonal vegetation change in the Chinese Loess Plateau since MIS 3. *Palaeogeography, Palaeoclimatology, Palaeoecology* **404**, 89–96.

Zijderveld, J.D.A., 1967. AC demagnetization of rocks: analysis of results. In: Collinson, D.W., Creer, K.M., Runcorn, S.K. (Eds.), *Methods in Paleomagnetism: Proceedings of the NATO Advanced Study Institute on Palaeomagnetic Methods held in the Physics Department of the University of Newcastle upon Tyne, April 1–10, 1964*. Elsevier Publishing Company, Amsterdam, London, New York, pp. 254–286.